



AMERICAN METEOROLOGICAL SOCIETY

Journal of Climate

EARLY ONLINE RELEASE

This is a preliminary PDF of the author-produced manuscript that has been peer-reviewed and accepted for publication. Since it is being posted so soon after acceptance, it has not yet been copyedited, formatted, or processed by AMS Publications. This preliminary version of the manuscript may be downloaded, distributed, and cited, but please be aware that there will be visual differences and possibly some content differences between this version and the final published version.

The DOI for this manuscript is doi: 10.1175/2008JCLI2261.1

The final published version of this manuscript will replace the preliminary version at the above DOI once it is available.



1 Tropical Pacific Climate and its Response to Global Warming in the Kiel Climate Model

2
3 W. Park, N. Keenlyside, M. Latif, A. Ströh

4 Leibniz-Institut für Meereswissenschaften, Kiel, Germany

5 R. Redler

6 NEC Laboratories Europe, NEC Europe Ltd., Sankt Augustin, Germany

7 E. Roeckner

8 Max-Planck-Institut für Meteorologie, Hamburg, Germany

9 G. Madec

10 LOCEAN, Institut Pierre Simon Laplace, Paris, France

11
12
13
14
15
16
17 J. Climate, submitted, 24th September 2007; revised 18th May 2008

18
19
20
21
22
23 _____
24 Corresponding author: Dr. Wonsun Park, Leibniz Institute of Marine Sciences (IFM-

25 GEOMAR), Duesternbrooker Weg 20, D-24105 Kiel, Germany

26 Email: wpark@ifm-geomar.de, Phone: +49-(0)431-600-4060, Fax: +49-(0)431-600-4052

27

Abstract

A new, non-flux corrected, global climate model is introduced, the Kiel Climate Model (KCM), which will be used to study internal climate variability from interannual to millennial time scales and climate predictability of the first and second kind. The version described here is a coarse resolution version that will be employed in extended-range integrations of several millennia. KCM's performance in the Tropical Pacific with respect to mean state, annual cycle, and El Niño/Southern Oscillation (ENSO) is described. Additionally, the Tropical Pacific response to global warming is studied.

Overall, climate drift in a multi-century control integration is small. However, KCM exhibits an equatorial cold bias at the surface of the order 1°C , while strong warm biases of several degrees are simulated in the eastern Tropical Pacific on both sides off the equator, with maxima near the coasts. The annual and semi-annual cycles are realistically simulated in the eastern and western equatorial Pacific, respectively. ENSO performance compares favorably to observations with respect to both amplitude and period.

An ensemble of eight greenhouse warming simulations was performed, in which the CO_2 concentration was increased by 1% per year until doubling was reached, and stabilized thereafter. Warming of equatorial Pacific sea surface temperature (SST) is, to first order, zonally symmetric and leads to a sharpening of the thermocline. ENSO variability increases due to global warming: During the 30 year period after CO_2 doubling, the ensemble mean standard deviation of Niño3 SST anomalies is increased by 26% relative to the control, and power in the ENSO band is almost doubled. The increased variability is due to both a strengthened (22%) thermocline feedback and an enhanced (52%) atmospheric sensitivity to SST, both are associated with changes in the basic state. Although variability increases in the mean, there is a large spread among ensemble members and hence a finite probability that in the "model world" no change in ENSO would be observed.

1 **1. Introduction**

2 Coupled air-sea feedbacks in the Tropical Pacific influence its annual mean state, annual
3 cycle, and interannual variability. For instance, the existence of an annual cycle in the eastern
4 equatorial Pacific, which is unexpected since the sun crosses the equator twice, is due to such
5 coupled interactions. Also, the El Niño/Southern Oscillation (ENSO) phenomenon, the most
6 pronounced interannual climate fluctuation, is an inherently coupled air-sea mode.
7 Furthermore, ENSO derives its predictability potential from its coupled nature.

8

9 The simulation of Tropical Pacific climate and its variability, however, has proven a challenge
10 for global climate models (e. g., Neelin et al. 1992; Latif et al. 1994; Achuta Rao and Sperber
11 2000; Latif et al. 2001; van Oldenburgh et al. 2005; Achuta Rao and Sperber 2006, Guilyardi
12 et al. 2006; Lin 2007). This is partly due to the presence of unstable air-sea interactions,
13 which tend to amplify biases in the individual model components. An important one is the
14 Bjerknes feedback (Bjerknes 1969; Neelin et al. 1998), which is a positive feedback between
15 the zonal wind stress, thermocline depth, and SST at the equator. Another example is the
16 cloud cover/SST feedback (Ma et al. 1996; Philander et al. 1996) in the eastern off-equatorial
17 oceans.

18

19 Apart from the feedbacks there are several other difficulties in simulating tropical Pacific
20 climate. The following is an in exhaustive list, but ones which we believe to be important.
21 Resolution matters and is often a limiting factor for a realistic simulation in both the ocean
22 and the atmosphere. The simulation of internal ocean waves (Busalacchi and O'Brien 1981),
23 which play an important role in ENSO dynamics (Schopf and Suarez 1988), and the narrow
24 equatorial and coastal upwelling zones require relatively high horizontal resolution in the
25 ocean that is often not affordable in global climate models.[0] Likewise, the steep orography
26 associated with the Andes affecting the local wind regimes that drive upwelling in the ocean
27 can be adequately resolved only using relatively high resolution in the atmosphere. Finally,

1 most global climate models do not resolve the Tropical Instability Waves, which contribute to
2 the ocean heat transport toward the equator, as described by Jochum et al. (2005). Resolving
3 Tropical Instability Waves may help to reduce the so called cold bias problem in the
4 equatorial Pacific, one of the most important problems in coupled ocean-atmosphere models
5 (Neelin et al. 1992; Latif et al. 2001).

6

7 In addition to being challenging, the Tropical Pacific is a welcome test bed for global climate
8 models and the employed physical parameterizations for several reasons. Examples are: first,
9 because coupled feedbacks are important. Second, because the internal timescales are small,
10 so that only relatively short integrations are required, third, because an observing system is in
11 place, the TOGA-TAO (Tropical Atmosphere-Ocean) array (McPhaden et al. 1990), which
12 enables quantitative model/data comparisons. Finally, because the socio-economic impacts of
13 Tropical Pacific variability, particularly ENSO, are large, requiring realistic simulation of not
14 only first but also higher statistical moments. There is a wide range of model behavior in the
15 Tropical Pacific that is reflected in both climatology and variability. This applies also to the
16 response of the Tropical Pacific to global warming (see, for instance, the recent studies by van
17 Oldenbrough et al. (2005) and Guilyardi (2006)). Even the change of the mean state in
18 response to global warming is not the same in all models. The Cane and Zebiak model
19 (Zebiak and Cane 1987), for instance, simulates a “La Niña-like” response, while most other
20 models simulate an “El Niño-like” change (Collins et al. 2005). Some models show a
21 weakening of the interannual variability, other models simulate an increase, and again other
22 models yield virtually no change. Theoretical studies show that the mean state has a strong
23 influence on ENSO statistics (Battisti and Hirst 1989), so that model biases may determine the
24 nature of the interannual variability and thus its response to global warming (Fedorov and
25 Philander 2000). Likewise, the decadal variability of the subtropical cells (STCs) is not well
26 captured by some climate models (Solomon and Zhang 2006) and their response to global

1 warming is highly uncertain, varying strongly from model to model, even with respect to sign
2 (Lohmann 2006, pers. communication).

3

4 Here we describe the first version of the Kiel Climate Model (KCM), a coupled ocean-
5 atmosphere-sea ice model that will serve as the dynamical core of the Earth system model
6 being developed at the Leibniz Institute of Marine Sciences. The model is effectively the next
7 generation of the SINTEX family (Scale INteractions Experiments; Navarra et al. 2003;
8 Gualdi et al. 2003; Guilyardi et al. 2003; Luo et al. 2005) of models, as each component has
9 been updated to the most recent version. This is the first paper describing KCM, and results
10 using a relatively coarse model resolution are presented, with a focus on the Tropical Pacific.

11 We compare KCM's performance to observations and contribute also to the discussion on the
12 Tropical Pacific response to global warming. Forthcoming papers will deal with lower-
13 frequency climate variations, specifically the multidecadal variations of the Atlantic
14 Meridional Overturning Circulation (MOC) and including its interaction with ENSO, and with
15 the extension of KCM by adding other components of the Earth system. Special emphasis will
16 be put on the coupling of ocean biogeochemistry and the investigation of the coupled
17 physical/ocean biogeochemistry response to global warming.

18

19 This paper is organized as follows. We describe the model and the experiments in section 2.
20 The mean state and the annual cycle simulated by KCM are compared to observations in
21 section 3. ENSO performance is discussed in section 4, while the Tropical Pacific response to
22 global warming is described in section 5. We conclude the paper with a brief summary and a
23 discussion of our main findings in section 6.

24

25 **2. Model and experiments**

26 KCM consists of the ECHAM5 (ECmwf HAMburg atmospheric general circulation model
27 version 5; Roeckner et al. 2003) atmospheric general circulation model (AGCM) coupled to

1 the NEMO (Nucleus for European Modeling of the Ocean; Madec et al. 1998; Madec 2008)
2 ocean-sea ice general circulation model, with the OASIS3 (Ocean Atmosphere Sea Ice Soil
3 version 3; Valcke 2006) coupler. No form of flux correction or anomaly coupling, either in
4 fresh water, heat, or wind stress is used. A brief description of the model components and the
5 experiments performed is now given; a schematic overview of the model is shown in Figure 1.

6

7 ECHAM5 is the latest version of the ECHAM model developed at the Max Planck Institute
8 for Meteorology (MPI). It is a spectral model employing state-of-the-art physics. A detailed
9 description of the model is given in Roeckner et al. (2003); a more concise summary of the
10 model can be found in Roeckner et al. (2006), where the sensitivity of results to resolution is
11 described. The model (as part of the MPI climate model) was used to carry out scenario
12 simulations for the IPCC (Intergovernmental Panel on Climate Change) 2007 fourth
13 assessment report (AR4; IPCC 2007). However, in contrast to the ECHAM5 model version
14 used by MPI in the IPCC AR4, we use the model's statistical cloud cover scheme (Tompkins
15 2002). In this scheme fractional cloudiness is calculated statistically, using a probability
16 density function for total water, as suggested from high-resolution cloud-resolving model
17 simulations of tropical deep convection.

18

19 NEMO (Madec et al. 1998; Madec 2008) consists of the OPA9 (Océan PARallélisé version 9)
20 ocean general circulation model (OGCM) and the LIM2 (Louvain-la-Neuve Ice Model
21 version 2) sea ice model. OPA9 is the most recent version of the OPA model developed at
22 LOCEAN - Institut Pierre Simon Laplace. OPA is widely applied in oceanography (research
23 and operational) and climate change studies. It is a z-coordinate OGCM that includes the most
24 recent developments in ocean modeling, such as partial bottom cells and a free surface
25 formulation. Details on most aspects of the model can be found in Madec (2008). Details on
26 sensitivity of the solution to partial cells and advections schemes is given by Barnier et al.
27 (2006), who also provide a concise summary of the model physics. LIM is a three level

1 dynamic-thermodynamic sea ice/snow model developed at Louvaine-la-Neuve (Fichefet and
2 Morales Maqueda 1997). Previous versions of both OPA and LIM, as part of a global coupled
3 models (INGV - Istituto Nazionale di Geofisica e Vulcanologia, IPSL - Institut Pierre Simon
4 Laplace), have contributed to the IPCC AR4 (IPCC 2007).

5

6 The coupling strategy in KCM is as follows: NEMO receives surface heat flux, fresh water
7 flux, and wind stress from ECHAM5 via OASIS3 coupler through a new technical interface
8 that was coded during the development of KCM and implemented in NEMO. The heat flux is
9 separated into a solar and non-solar part, and calculated separately over water and sea ice. In
10 addition and for the sake of numerical stability of the sea ice model, the derivative of non-
11 solar heat flux with respect to surface temperature is passed. Net fresh water flux
12 (precipitation minus evaporation) includes river runoff and glacier calving, both of which are
13 provided by ECHAM5's hydrological model. Snow fall is passed additionally to be used for
14 the sea ice model. Sea surface temperature, surface ocean velocity, sea ice fraction, sea ice
15 temperature, sea ice thickness, and snow thickness are transferred from NEMO to the
16 ECHAM5 atmosphere model via the coupler. These physical fields are used for calculation of
17 heat, freshwater, and momentum fluxes in the atmosphere. Sea ice dynamics and
18 thermodynamics are calculated inside of the sea ice model every five ocean time steps. The
19 coupling interval between the ocean and atmosphere is once per day. In the KCM simulations
20 described here, the atmospheric resolution is T31 ($3.75^\circ \times 3.75^\circ$) horizontally with 19 vertical
21 levels. The horizontal ocean resolution is based on a 2° Mercator mesh and is on average 1.3° ,
22 with enhanced meridional resolution of 0.5° close to the equator (ORCA2), and with 31 levels
23 in the vertical. OASIS3 coupler interpolates the exchange fields described above to and from
24 source and target model grids.

25

26 Here we analyze two experiments: a 20th century equivalent (20C) control experiment that
27 assumes “present day” values for greenhouse gases ($\text{CO}_2=348$ ppm) and a series of eight 100

1 year long global warming simulations (21st century equivalent, 21C). In the latter, CO₂
2 concentration is increased at 1% per year (compound) till CO₂ doubling is reached, after about
3 70 years, and stabilized thereafter for another 30 years. The 20C control simulation is 430
4 years long, but only the last 330 years are analyzed here. The initial conditions are taken from
5 a long (500 year) coupled model simulation, with different parameter values. This spin-up run
6 started from the Levitus (1998) climatology. The 21C global warming experiments were
7 started from initial conditions chosen semi-regularly with 30 or 40 year intervals from the 20C
8 control run (Fig. 2).

9

10 **3. Climatology**

11 The model climate is relatively stable, as illustrated by the simulated globally averaged 2-m
12 air temperature (SAT; Fig. 2). The global mean temperature averaged over the length of the
13 simulation equals $14.24 \pm 0.15^{\circ}\text{C}$, which compares well with the observed surface air
14 temperature mean over the period 1971-2004 of $13.91 \pm 0.20^{\circ}\text{C}$ from NCEP/NCAR reanalysis
15 (Kalnay et al. 1996). The mean SST bias pattern calculated from last 100 years of the control
16 experiment (Fig. 3) compares favorably to those simulated by other state-of-the-art coupled
17 global climate models (CGCMs) (Latif et al. 2001), particularly given the low resolution in
18 the atmosphere. A common problem is seen in the North Atlantic, where SSTs are up to 9°C
19 too cold. This bias is most likely due to a too southward flowing and diffusive North Atlantic
20 Current, but may also be due to deficiencies in the atmosphere such as in the storm track
21 position. In the Tropics biases are generally not greater than 1°C, except for the warm biases
22 along the east coast of South America, North America, and Africa. The latter biases are
23 common to many CGCMs, and are partly due to the incorrect representation of stratocumulus
24 clouds and coastal upwelling, as was inferred from uncoupled integrations with the respective
25 model components. The problem is particularly acute in the Tropical Atlantic where, as in
26 most other models (Davey et al. 2002), the warm bias extends across most of the basin and
27 reverses the zonal SST gradient along the equator.

1

2 In the Tropical Pacific, the area of focus for the remainder of the paper, the SST biases are
3 smaller than in many state-of-the-art CGCMs (Guilyardi 2006): SSTs in the equatorial cold
4 tongue are about 1°C too low (Fig. 3); averaged over the Niño3 region (150 - 90°W, 5°S -
5 5°N) simulated SST equals 25.22°C, while the observed value is 25.69°C (1870-2004,
6 HadISST (Rayner et al. 2003)). The equatorial cold bias is associated with too strong surface
7 zonal wind stress (Figs. 4a, b), as compared to the NCEP/NCAR reanalysis (Kalnay et al.
8 1996); averaged over the Niño4 region (160°E - 150°W, 5°S - 5°N) simulated zonal wind
9 stress is -0.052Pa, which is larger than that of many models (Guilyardi 2006) and the
10 NCEP/NCAR reanalysis (-0.029Pa). Maximum wind stress curl is located more northward
11 than in observations, and the strength is enhanced in the model (Figs. 4c, d). KCM produces
12 more precipitation than observed in the convergence zones and the rainfall maxima are shifted
13 somewhat poleward (Figs. 4e, f). The South Pacific Convergence Zone (SPCZ), which is
14 oriented in a North-West South-East direction in observations, is more zonally orientated in
15 the model and extends too far east. Nevertheless the model produces a reasonable overall
16 distribution. The equatorial thermocline (Fig. 5a) is well simulated: The east-west slope is
17 only slightly stronger than in observations (Fig. 5b), which results from the overly strong
18 equatorial surface zonal wind stress. Common to many ocean models, the simulated
19 thermocline is too diffusive. The simulated 20°C isotherm depth (Z_{20}) along the equator is
20 comparable to the observations, while it is shallower than observed in the Subtropics (Figs. 5c,
21 d).

22

23 The model simulates both tropical and subtropical cells (Fig. 5e) that agree with results from a
24 forced simulation (Fig. 5f) of the ocean component of the coupled model, NEMO, driven with
25 CORE (Large and Yeager 2004) forcing. The meridional (zonally integrated) upper ocean
26 circulation is expressed by the overturning streamfunction, Ψ . The subtropical cell strengths
27 of the coupled and uncoupled runs are very similar in the south, while the northern circulation

1 is approximately 30% stronger in the coupled model simulation. The latter difference is due to
2 stronger surface wind stress (curl) in the coupled model, as described above.

3

4 The simulated annual cycle in the eastern Pacific along the equator, shown as deviation from
5 the annual mean (Fig. 6a), agrees quite well with observations (Rayner et al. 2003) (Fig. 6b)
6 in terms of strength and westward phase propagation; this is not the case in many other
7 models (Latif et al., 2001). In terms of phase, the simulated annual cycle in the east lags the
8 observed one by a month: SSTs are warmest (coldest) in April (September/October) in KCM
9 as compared to March (August/September) in observations. In the western and parts of the
10 central Equatorial Pacific, the model correctly captures the observed semi-annual cycle in
11 terms of phase. The simulated semi-annual cycle is, however, mostly overestimated: the
12 model SST near the dateline, for instance, varies by more than $\pm 0.5^{\circ}\text{C}$, whereas the observed
13 variations are much smaller and attain appreciable magnitude only in a rather small region in
14 the very western Pacific, where in turn the model variability is much too weak.

15

16 **4. ENSO variability**

17 In the previous section, it was shown that KCM realistically simulates important aspects of
18 the mean Tropical Pacific climate and the annual cycle, both of which are believed to be
19 important for ENSO. In accord with this the model simulates Tropical Pacific SST interannual
20 variability reasonably. The spatial pattern of the standard deviation agrees reasonably well
21 with observations (Fig. 7). However, KCM produces stronger equatorial SST variability than
22 observed, specifically over the western and central equatorial Pacific and too weak variability
23 near the eastern coast south of 15°S . A band of too strong variability is simulated in the
24 northern Subtropics.

25

26 Simulated Niño3 averaged SST anomalies show clear similarities to observations (Figs. 8a,
27 b). In particular, both have similar amplitude, with the standard deviations of the observed and

1 simulated time series being 0.78 and 0.93 (see Table 1), respectively. Both time series are also
2 quite irregular, with phases of weaker variability broken by a series of stronger events, and
3 have similar spectral characteristics (Fig. 8c). As in observations, the model's dominant
4 spectral peak is at four years. In the model, however, there is greater (less) power in the two-
5 to-four (four-to-five) year band compared to observations. This tendency is further enhanced
6 when the statistical cloud cover scheme is not used. Observed and simulated distributions
7 (histograms) of Niño3 SST anomalies also agree quite well (see Fig. 16a). However, the
8 occupancy of values close to zero is less in the simulated time series than in observations, and
9 the skewness (kurtosis) of the simulated time series amounts to 0.04 (2.95), which does not
10 correspond well with the observed value of 0.75 (4.13) (Table 1). Furthermore, the observed
11 strong phase locking of ENSO to the annual cycle is not captured by KCM: The model
12 simulates a weak semi-annual cycle in Niño3 SST variability (Fig. 8d), with peaks in
13 January/February and July/August, as compared to the pronounced annual cycle in
14 observations, with peak values in December/January and a minimum value in April. This is
15 somewhat surprising, as the SST annual cycle in the eastern equatorial Pacific is quite well
16 simulated by KCM. However, as described above the semi-annual cycle in SST is relatively
17 strong near the dateline and the SST annual cycle in the east lags the observations by one
18 month. Both may contribute to the problem, which will be the subject of future investigation.

19

20 Hovmoeller diagrams of anomalies in zonal surface wind, 20°C isotherm depth (a measure of
21 upper ocean heat content) and SST along the equator (Fig 9) show key similarities to
22 observations. First, prior to El Niño events there is a build up of equatorial heat content. This
23 is most clearly seen by the positive heat content anomalies in the west (Fig. 9b). These
24 anomalies propagate eastward, strengthening as they go. They lead to SST anomalies in the
25 eastern Pacific (Fig. 9c) that are associated with westerly wind anomalies over the western
26 and central Pacific (Fig 9a), indicating remote wind stress forcing. The lag correlation
27 between warm water volume (WWV) integrated over the tropical Pacific (120°E-80°W, 5°S-

1 5°N) are maximum when WWV leads Niño3 SST anomalies by seven months (not shown);
2 the maximum correlation in the model (0.6) is slightly weaker than in observations (0.7).
3 Thus, the dynamics of the simulated ENSO appear to be in agreement with the recharge-
4 discharge theory of Jin (1997), and suggest the dominance of the thermocline feedback in the
5 model.

6

7 The Hovmoeller diagrams also suggest an SST-mode character to the ENSO variability: in
8 particular, SST anomalies clearly propagate westward, although there are some hints of
9 eastward propagation in the zonal wind. In observations, both eastward and westward
10 propagation of SST anomalies is found, with indications that weak (strong) events propagate
11 westward (eastward). Results from theoretical work argue that these changes in east-west
12 propagation characteristics reflect shifts from a more thermocline driven subsurface mode to a
13 more SST-zonal current driven surface mode (Fedorov and Philander 2001). In the model it
14 appears that the SST mode-component is stronger than that in observations. Nonetheless, the
15 results suggest the thermocline feedback dominates in KCM, because the zonal winds do not
16 exhibit the characteristics of an SST mode being dominated by stationary anomalies in the
17 west. Furthermore, as pointed out by Neelin et al. (1994), ENSO in the real world is most
18 likely a mixed surface/subsurface dynamics mode that involves elements of both extreme
19 cases.

20

21 Several other features are noteworthy in the Hovmoeller diagrams. First, in difference to
22 observations, simulated SST anomalies (Fig. 9c) are generally stronger in the central Pacific,
23 rather than in the east (Fig. 9f). Second, as seen in observations and already mentioned above,
24 the model realistically simulates quiescent periods. Third, superimposed on the slow ENSO
25 variability, a great deal of intra-seasonal variability is seen in the wind, 20°C-isotherm depth,
26 and SST variability. This variability may contribute to the realistic irregular nature of the
27 simulated ENSO variability.

1 Finally, the ENSO global teleconnection pattern is investigated. The regression of simulated
2 monthly Niño3 SST anomalies onto sea level pressure anomalies shows the clear Southern
3 Oscillation seesaw pattern over the tropics, which corresponds quite well to observations (Fig.
4 10). Explained variance over the eastern tropical Pacific is greater than 30% in the simulation,
5 slightly lower than that of observation (40%). However, the meridional width is narrower in
6 the model. The teleconnection to Northern and Southern Hemisphere extra-tropics compares
7 quite well to observations, although the teleconnection to the Northern (Southern) Hemisphere
8 maybe overestimated (underestimated). However, one has to keep in mind that the
9 observational data is much shorter than that of the model. Thus, KCM is able to realistically
10 simulate ENSO dynamics and capture the major atmospheric teleconnection patterns.

11

12 **5. Response to global warming**

13

14 *Change of mean state*

15 As described above, KCM simulates Tropical Pacific climate and variability reasonably well.
16 The response of both to global warming (see section 2) is now described. Global mean surface
17 air temperature (SAT) changes in the 21C (21st century equivalent) greenhouse warming
18 simulations are shown in Figure 2 together with SAT simulated in the control simulation.
19 Allowing for the inertia of the climate system, global mean SAT increases rather linearly with
20 respect to CO₂ concentration until the time of CO₂ doubling. Although CO₂ concentration is
21 fixed after doubling is reached, the global mean SAT still increases, but at a slower rate. We
22 note, however, that equilibrium was not reached at the end of the 21C simulations. The
23 transient climate response (TCR; Cubasch et al. 2001), defined as the global mean surface air
24 temperature change averaged over a 20-year period centered at the time of CO₂ doubling
25 (years from 61 to 80), is 2.9°C, which is stronger than those (1.2 - 2.6°C) of the IPCC models
26 (Table 8.2 in IPCC 2007).

27

1 The ensemble mean surface temperature response pattern is shown in Fig. 11, defined as the
2 difference between the last 30 years of the 21C integrations and the control simulation.
3 Consistent with virtually all climate models, a strong land-sea contrast is simulated by KCM.
4 The warming exceeds 6°C in the high latitudes of the Northern Hemisphere, specifically over
5 parts of Eurasia and North America. Over the North Atlantic Ocean, the warming is rather
6 small on average, with a small region of cooling near 50°N due to a substantial weakening of
7 the MOC. The warming over the Southern Ocean is also rather weak, in accord with most
8 other climate models.

9

10 The equatorial Pacific surface temperature increases by about 3°C, which is generally higher
11 than the warming over the subtropical and mid-latitude Pacific Ocean. One important
12 exception is the north western subtropical Pacific, where the warming attains a similar
13 strength. We shall return to this point below when discussing the changes in the subtropical
14 cells. Although slightly stronger in the west, the warming at the equator is almost zonally
15 symmetric: Maximum warming in the east and west are 3.0°C and 3.2°C, respectively. In
16 terms of the ‘ENSO-ness’ index, defined as the pattern correlation between the SST trend and
17 first EOF of SST anomalies in the equatorial region (120°E-80°W, 10°S-10°N), our change
18 equals 0.3, which corresponds to a weakly “El Niño-like” response and is smaller than that of
19 most models (Fig 10.16 in IPCC 2007). In the vertical, the temperature increase is larger near
20 the surface and less pronounced in deeper levels (Fig. 12a), which enhances the vertical
21 gradient in the region of the thermocline (Fig. 5a) and thus sharpens it. The sharpness of the
22 thermocline is an important parameter controlling ENSO characteristics (Fedorov and
23 Philander 2001; Meehl et al. 2001), and as described below, contributes to the changes in
24 ENSO simulated in response to global warming.

25

26 The zonal wind stress is reduced over the western and eastern equatorial Pacific, while it is
27 increased over the central equatorial Pacific (Fig. 12c). A reduced equatorial zonal wind stress,

1 i.e. weakened Trade Winds, weakens the Ekman transport divergence and hence the equatorial
 2 upwelling, which as a consequence is responsible for the enhanced warming over the western
 3 and eastern parts. The stronger zonal wind stress over the central part, on the other hand,
 4 enhances upwelling, which explains the local minimum of warming in this region. The Z_{20}
 5 (20°C isotherm depth) along the equator increases by 9m on average, with a slightly larger
 6 increase in the west and east of around 15m, due to surface warming and weakened upwelling
 7 (Fig. 12d). The equatorial wind stress changes discussed above are also reflected in the
 8 isotherm depth changes. The isotherm depth becomes shallower around 5°N in the longitude
 9 band $160^{\circ}\text{-}120^{\circ}\text{W}$, and in the region $5^{\circ}\text{-}10^{\circ}\text{S}$ in the band $180^{\circ}\text{-}110^{\circ}\text{W}$. The response of the
 10 wind stress curl on both hemispheres is quite patchy (Fig. 12c), but is negative when
 11 integrated zonally over the Pacific basin (not shown).

12

13 Figure 12b shows the response pattern of the meridional overturning streamfunction, Ψ , which
 14 is quite complicated. To ease interpretation Figure 13 displays the time evolutions of the
 15 tropical (TCs) and subtropical cells (STCs) from the control simulation and the ensemble of
 16 CO_2 experiments. TC and STC indices are defined according to Lohmann and Latif (2005) by
 17 the zonally averaged Pacific meridional overturning streamfunction, Ψ , as:

18

19
$$\text{TC} = [\Psi_{\text{max}}(5^{\circ}\text{S}\text{-}5^{\circ}\text{N}, \text{upper } 250\text{m}) - \Psi_{\text{min}}(5^{\circ}\text{S}\text{-}5^{\circ}\text{N}, \text{upper } 250\text{m})]$$
 and

20
$$\text{STC} = [\Psi_{\text{max}}(10^{\circ}\text{N}\text{-}30^{\circ}\text{N}, \text{upper } 250\text{m}) - \Psi_{\text{min}}(10^{\circ}\text{S}\text{-}30^{\circ}\text{S}, \text{upper } 250\text{m})]$$

21

22 TC strength is clearly reduced by about 10% on average in the 21C integrations (Fig. 13a),
 23 most likely due to the changes in equatorial zonal wind stress described above. STC strength,
 24 however, is not significantly changed (Fig. 13b). Yet, when we separate STC strength into its
 25 Northern and Southern Hemisphere components, considerable changes become apparent.
 26 While the Northern Hemisphere cell is reduced (Fig. 13c), the Southern Hemisphere cell is
 27 strengthened relative to the control run (Fig. 13d). Please note the different signs of the

1 northern and southern cells in terms of the streamfunction. Thus both cells respond to global
2 warming, but there is a strong cancellation between the changes in the two cells, so that the
3 net change is very small. The spatial response pattern of the overturning (Fig. 12b) indicates a
4 shallow Southern Hemisphere and a deep Northern Hemisphere cell response.

5

6 We can understand the northern and southern STC responses by the SST and wind stress curl
7 changes (Figs. 11, 12c). As already noted above, the northern Subtropics exhibit relatively
8 strong warming in the west and central part. In contrast, the eastern and central southern
9 Subtropics show a much reduced warming. The different SST response can be explained by
10 the changes in the Trade Winds of both hemispheres. While they strengthen in the south
11 eastern subtropical Pacific, they weaken in the north western Pacific (Fig. 12c), changing
12 surface wind speed, evaporation, and vertical mixing in the ocean. The opposite changes in
13 evaporation and vertical mixing in the northern and southern subtropics explain the different
14 SST response in these two regions. Thus as density in low latitudes is mostly temperature-
15 driven, the warming (cooling) in the northern (southern) subtropics implies reduced
16 (enhanced) forcing of the northern (southern) STC. Furthermore, the response in the zonally
17 integrated wind stress curl near 10°N and 10°S (not shown) is negative and thus also
18 contributes to the hemispheric differences in the STC response. The mechanism behind the
19 STC changes in KCM, however, may not act in other models.

20

21 *Change of ENSO*

22 Figure 14 shows the evolution of Niño3 SST anomalies from the eight 21C experiments with
23 different initial conditions. The ensemble mean temperature evolution in the Niño3 region
24 smoothed with a 10 year running mean filter shows a clear increase of about 3°C, with some
25 tendency for equilibration towards the end of the integrations. Interannual variability also
26 increases in the second half of the integrations. The ensemble mean standard deviation of
27 Niño3 averaged SST anomalies for the last 30 years is 1.15°C. This represents a 26% increase

1 from that of the 20C control simulation (0.91) and is well outside one standard deviation
2 confidence interval (Table 1). The response, however, varies quite strongly among the
3 ensemble members. Spectral analysis was performed to identify the response in the frequency
4 domain (Fig. 15). To account for the inertia of the coupled system, spectra were calculated
5 from the last 30 years of the 21C integrations. They were calculated for each realization, and
6 then averaged to obtain an ensemble mean spectrum. A spectrum for the 20C control
7 simulation was calculated similarly, by taking eight 30 year chunks from the run with no
8 overlap. We note that the control run spectrum obtained from the eight overlapping 30 year
9 chunks is very similar to the spectrum shown in Fig. 8c determined from the full 330 year
10 long control simulation. One standard deviation of the ensemble spread is used here as a
11 rough uncertainty estimate for both the 20C and 21C simulations. The ensemble mean
12 spectrum of the 21C integrations displays an increase in variability that is most pronounced at
13 interannual time scales (Fig. 15). At the ENSO peak period of about 4 years, the increase in
14 power amounts to double. The overall shape of the spectrum does not change much, and the
15 ENSO period remains almost constant at about 4 years, although a small shift to a longer
16 period is simulated. Finally, ENSO remains a broad-band phenomenon in the frequency
17 domain in the 21C integrations. We did not assess the statistical significance of the results, but
18 the pure fact that the change extends over the whole frequency domain is not expected only
19 due to sampling errors. We note however, that an ensemble of reasonable size is needed to
20 detect the changes in variability: not every individual ensemble member does show an
21 obvious increase as indicated by the large range given by the red bars in Figure 15.

22

23 We next compute histograms of the simulated Niño3 SST anomalies in order to study possible
24 changes in distribution. The distribution becomes wider in the 21C integrations indicating an
25 overall enhanced variability. Of particular interest are the changes at the tails, as they
26 represent the extreme events. As can be seen from the time series (Fig. 14) both extreme
27 warm and cold events become more frequent (Fig. 16a), with stronger changes in the warm

1 extremes. This is reflected in the skewness which is slightly increased from -0.03 ± 0.21 in 20C
 2 to 0.28 ± 0.39 in 21C (Table 1). The kurtosis changes from 2.60 ± 0.31 to 3.60 ± 0.87 . The
 3 corresponding values for skewness and kurtosis in the observations are 0.75 and 4.13 (Table
 4 1), respectively. Clearly, KCM's skewness and kurtosis are considerably lower than those
 5 obtained from observations, which indicates a too symmetric and not peaked enough
 6 distribution. Thus, it is debatable as to whether the changes in the higher moments of the
 7 distribution are reliable given the large biases.

8

9 Table 1. Basic statistics of Niño3 SST anomalies. Confidence interval represents one standard
 10 deviation of the eight ensemble members.

| | Observation | 20C | | 21C |
|--------------------|-------------------------|--------|------------------|-----------------|
| | (HadISST, 1870-2004) | 330yrs | 30yr chunks | |
| standard deviation | 0.78 | 0.93 | 0.91 ± 0.15 | 1.15 ± 0.27 |
| skewness | 0.75 | 0.04 | -0.03 ± 0.21 | 0.28 ± 0.39 |
| kurtosis | 4.13 | 2.95 | 2.60 ± 0.31 | 3.60 ± 0.87 |

11

12 Finally, in order to understand the reasons for the increase in ENSO variability we studied the
 13 response of the annual cycle in the eastern Equatorial Pacific and also the changes in ocean-
 14 atmosphere feedbacks. As observed ENSO variability is phase locked to the annual cycle,
 15 changes in the annual cycle may impact ENSO amplitude and frequency (Chang et al. 1995;
 16 Liu 2002). The annual cycle response of Niño3 SST shows a slight weakening (Fig. 16b). As
 17 the change is small and given the poor phase locking of ENSO to the annual cycle in the
 18 model, it seems unlikely that this change has any significant effect on KCM's ENSO response.

19

20 The four most important feedbacks for ENSO are the thermocline and zonal advective
 21 feedbacks, atmospheric response to SST, and thermal damping. Changes in these, which are

1 largely controlled by changes in the mean state, impact ENSO variability (amplitude, period,
2 and structure). Changes in the zonal advective feedback were not investigated in detail, but as
3 the zonal asymmetry of the basic state did not change much (Fig. 11) and the westward
4 propagation of equatorial SST anomalies remained similar (not shown), they appear to be of
5 second order importance. Changes in the other feedbacks were estimated by linear regression.
6 As above, the analysis was performed on eight 30-year chunks from 20C and 21C simulations.
7 The thermocline feedback, estimated from the SST/20°C isotherm depth relation for the Niño3
8 region, increases by 22% (Fig. 17a,b). The increased sensitivity of SST to subsurface
9 temperature anomalies is consistent with the sharper thermocline (Fig. 12a) and increased
10 upwelling due to the strengthened Trades (Fig. 12c) in the 21C warming simulations. The
11 atmospheric response to SST anomalies, estimated from the relation between Niño4 zonal
12 wind stress and Niño3 SST, increases by 52% (Fig. 17c,d). The enhanced atmospheric
13 sensitivity is likely due to the warmer atmospheric conditions, which supports an enhanced
14 hydrological cycle. The thermal damping feedback, estimated from the net surface heat
15 flux/SST relation for the Niño3 region, becomes important in the 21C experiments (not
16 shown). In the 20C control experiment the feedback is weak and couldn't be reliably
17 estimated. Thus, the enhanced ENSO variability in the greenhouse experiments results from
18 both the strengthening of the thermocline feedback and enhanced atmospheric sensitivity to
19 SST.

20

21 **6. Summary and discussion**

22 In this paper we introduced the newly developed Kiel Climate Model (KCM), described its
23 performance in the Tropical Pacific and response to global warming. Overall, the model's
24 performance is reasonable, despite not using flux correction, and similar to that of other state-
25 of-the-art global climate models, although we use relatively low resolution. However, as in
26 most other global climate models three main systematic errors are of major concern. First,
27 northern mid-latitude surface temperature is much too cold; second, the eastern tropical and

1 subtropical oceans are much too warm; and third, the phase locking of ENSO to the annual
2 cycle is not well captured. The latter indicates, together with the inability of the model to
3 simulate a reasonable skewness of eastern equatorial Pacific SST anomalies, that KCM's
4 ENSO dynamics are too linear. In spite of these deficiencies, the simulation of the annual
5 cycle in the eastern equatorial Pacific and ENSO are quite good, with only small differences
6 to observations. This is encouraging and we hope that KCM will become a useful tool to
7 study climate variability, up to timescales of millennia, and predictability of the first and
8 second kind, and to serve as kernel for the development of an Earth system model. Much
9 work, however, remains to reduce the biases described. This, however, is a long-term task.
10 We have to find a trade off between model resolution and systematic errors, because computer
11 resources are still rather limited and enable only relatively short integrations at very high
12 resolution. Physical parameterizations of unresolved processes can still be improved, and this
13 is an attractive research area requiring deep insight into the underlying physics. We shall
14 follow this latter route and increase of resolution is not our priority.

15

16 One of the major findings of this work is the intensification of ENSO in response to
17 greenhouse warming, as simulated in a series of eight experiments with increasing CO₂
18 concentration at 1% per year until doubling and then held constant. The ensemble mean
19 standard deviation of Niño3 SST anomalies increases by 26% in the 30 years after CO₂
20 doubling, while there is a doubling in power at the dominant ENSO period of 4 years. The
21 increase in ENSO variability was driven by a 22% strengthening of the thermocline feedback
22 and a 52% enhancement of atmospheric sensitivity to SST. The thermocline feedback
23 enhancement results from a sharper thermocline and increased upwelling. The increase in
24 atmospheric sensitivity may result from the warm atmospheric conditions, which drive an
25 enhanced hydrological cycle. Although the ensemble mean changes in ENSO variability are
26 large, there is quite some spread among ensemble members. This argues that climate change
27 studies of ENSO should be probabilistic.

1
2 Timmermann et al. (1999) also found an enhancement of the thermocline feedback due to a
3 sharpening of the thermocline. They used ECHAM4, the predecessor model of the ECHAM
4 version used here, coupled to a completely different (isopycnal) ocean model. In contrast to
5 Timmermann et al. (1999), the skewness in KCM changes in the opposite sense, such that
6 extreme warm events become more frequent as opposed to extreme cold events. Several
7 models do simulate enhanced interannual variability in response to global warming (van
8 Oldenbourgh et al. 2005; Guilyardi 2006), but there is still considerable spread among the
9 different models. Since a number of feedbacks are involved in the ENSO response to global
10 warming, the mean state in the Tropical Pacific should be well simulated, as the large biases
11 reduce confidence in the models. We do not know, for instance, as to whether the zonally
12 symmetric response of the mean state in KCM affects the ENSO response. Furthermore, at
13 this stage of analysis we do not know either as to whether the enhanced interannual variability
14 is a transient phenomenon. The response time of the subsurface ocean is much longer than
15 that of the surface ocean, which may lead to some additional warming at deeper levels thereby
16 counteracting the surface layer effects. Thus a much longer stabilization phase is needed to
17 obtain an equilibrium response. Nevertheless, the real ocean may behave in a similar way, so
18 that a transient increase in interannual variability is quite possible during this century, if
19 greenhouse gas emissions are not strongly reduced.

20

21 **Acknowledgements**

22 We would like to thank the Max-Planck-Institut für Meteorologie and LOCEAN - Institut
23 Pierre Simon Laplace for generously providing ECHAM5 and NEMO, respectively. We
24 would like to thank M. Schneiert for providing standalone NEMO simulation. Discussions
25 with J. Jungclaus, M. Esch, L. Kornblueh, and S. Hagemann on ECHAM5; V. Gayler, S.
26 Legutke, E. Maisonnave, and S. Valcke on OASIS3; and the DRAKKAR group, A. Biastoch,
27 and S. Masson on NEMO were very helpful during the model development. This work was

1 supported by the European Union's projects ENSEMBLES (GOCE-CT-2003- 505539) and
2 DYNAMITE (Contract 003903). The model integrations were performed at the Deutsches
3 Klimarechenzentrum and the Computer Centre at Kiel University.

4

1 **References**

2 Achuta Rao, K. and K. R. Sperber, 2000: El Niño Southern Oscillation in coupled models.
3 PCMDI Rep. 61, PCMDI, Lawrence Livermore National Laboratory, Livermore 95440, USA.

4

5 Achuta Rao, K. and K. R. Sperber, 2006: ENSO simulation in coupled ocean-atmosphere
6 models: are the current models better? *Climate Dyn.*, **27**, 1–15 DOI 10.1007/s00382-006-
7 0119-7.

8

9 Barnier, B., G. Madec, T. Penduff, J.-M. Molines, A.-M. Tréguier, J. Le Sommer, A.
10 Beckmann, A. Biastoch, C. Böning, J. Dengg, C. Derval, E. Durand, S. Gulev, E. Rémy, C.
11 Talandier, S. Theetten, M. E. Maltrud, J. McClean and B. De Cuevas, 2006 : Impact of partial
12 steps and momentum advection schemes in a global ocean circulation model at eddy-
13 permitting resolution. *Ocean Dyn.*, **56** (5-6), 543-567.

14

15 Battisti, D. S. and A. C. Hirst, 1989: Interannual variability in a tropical atmosphere–ocean
16 model: Influence of the basic state, ocean geometry, and nonlinearity. *J. Atmos. Sci.*, **46**,
17 1687–1712.

18

19 Bjerknes, J., 1969: Atmospheric teleconnections from the equatorial Pacific. *Mon. Wea. Rev.*,
20 **97**, 163-172.

21

22 Busalacchi, A. J. and J. J. O'Brien, 1981: Interannual Variability of the Equatorial Pacific in
23 the 1960's, *J. Geophys. Res.*, **86**, 10,901-10,907.

24

25 Chang, P., L. Ji, B. Wang, and T. Li, 1995: Interactions between the Seasonal Cycle and El
26 Niño-Southern Oscillation in an Intermediate Coupled Ocean-Atmosphere Model. *J. Atmos.*
27 *Sci.*, **52**, 2353–2372.

1
2
3
4
5
6
7
8
9
10
11
12
13
14
15
16
17
18
19
20
21
22
23
24
25
26
27

Collins, M., and The CMIP Modelling Groups, 2005: El Niño- or La Niña-like climate change? *Climate Dyn.*, **24**, 89–104 DOI 10.1007/s00382-004-0478-x

Cubasch, U., et al., 2001: Projections of future climate changes. In: *Climate Change 2001: The Scientific Basis. Contribution of Working Group I to the Third Assessment Report of the Intergovernmental Panel on Climate Change [Houghton, J.T., et al. (eds.)]*. Cambridge University Press, Cambridge, United Kingdom and New York, NY, USA, pp. 525–582.

Davey, M. K., M. Huddleston, K. Sperber, P. Braconnot, F. Bryan, D. Chen, R. Colman, C. Cooper, U. Cubasch, P. Delecluse, D. DeWitt, L. Fairhead, G. Flato, C. Gordon, T. Hogan, M. Ji, M. Kimoto, A. Kitoh, T. Knutson, M. Latif, H. Le Treut, T. Li, S. Manabe, C. Mechoso, G. Meehl, S. Power, E. Roeckner, L. Terray, A. Vintzileos, R. Voss, B. Wang, W. Washington, I. Yoshikawa, J. Yu, S. Yukimoto, and S. Zebiak, 2002: STOIC: A study of coupled model climatology and variability in tropical ocean regions. *Climate Dyn.*, **18**, 403–420.

Fedorov, A. V. and S.G.H. Philander, 2000: Is El Niño changing? *Science*, **288**, 1997–2002.

Fedorov, A.V., and S.G. Philander, 2001: A Stability Analysis of Tropical Ocean–Atmosphere Interactions: Bridging Measurements and Theory for El Niño. *J. Climate*, **14**, 3086–3101.

Fichefet, T. and M.A. Morales Maqueda, 1997: Sensitivity of a global sea ice model to the treatment of ice thermodynamics and dynamics. *J. Geophys. Res.*, **102**, 12, 609–12,646.

Gualdi, S., E. Guilyardi, A. Navarra, S. Masina, and P. Delecluse, 2003: The interannual variability in the tropical Indian Ocean as simulated by a CGCM. *Climate Dyn.*, **10**, 567–582.

1
2
3
4
5
6
7
8
9
10
11
12
13
14
15
16
17
18
19
20
21
22
23
24
25
26
27

Guilyardi E., P. Delecluse, S. Gualdi and A. Navarra, 2003: Mechanisms for ENSO phase change in a coupled GCM. *J. Climate*, **16**, 1141-1158.

Guilyardi, E., 2006: El Niño-mean state-seasonal cycle interactions in a multi-model ensemble. *Climate Dyn.*, **26**, 329-348.

Guilyardi, E., S. Gualdi, J. M. Slingo, A. Navarra, P. Delecluse, J. Cole, G. Madec, M. Roberts, M. Latif and L. Terray, 2004 : Representing El Niño in Coupled Ocean-Atmosphere GCMs: The Dominant Role of the Atmospheric Component. *J. Climate*, **17**, 24, 4623-4629, doi:10.1175/JCLI-3260.1.

IPCC, 2007: Climate Change 2007: *The Physical Science Basis. Contribution of Working Group I to the Fourth Assessment Report of the Intergovernmental Panel on Climate Change* [Solomon, S., D. Qin, M. Manning, Z. Chen, M. Marquis, K.B. Averyt, M. Tignor and H.L. Miller (eds.)]. Cambridge University Press, Cambridge, United Kingdom and New York, NY, USA, 996 pp.

Jin, F. F., 1997: An Equatorial ocean recharge paradigm for ENSO. Part I: Conceptual model. *J. Atmos. Sci.*, **54**, 811–829.

Jochum, M., R. Murtugudde, R. Ferrari, and P. Malanotte-Rizzoli, 2005: The impact of horizontal resolution on the equatorial mixed layer heat budget in ocean general circulation models. *J. Climate*, **18**, 841–851

Kalnay, E., M. Kanamitsu, R. Kistler, W. Collins, D. Deaven, L. Gandin, M. Iredell, S. Saha, G. White, J. Woollen, Y. Zhu, A. Leetmaa, B. Reynolds, M. Chelliah, W. Ebisuzaki, W.

1 Higgins, J. Janowiak, K. Mo, C. Ropelewski, J. Wang, R. Jenne, and D. Joseph, 1996: The
2 NCEP/NCAR 40-Year Reanalysis Project. *Bull. Amer. Meteor. Soc.*, **77**, 437–471.
3
4 Large, W. G. and S. G. Yeager, 2004: Diurnal to decadal global forcing for ocean and sea-ice
5 models: The data sets and flux climatologies. NCAR Tech. Note, NCAR/TN-460+STR, 111
6 pp. [Available online at <http://www.cgd.ucar.edu/oce/pubs/04pubs.html>].
7
8 Latif, M., E. Roeckner, M. Botzet, M. Esch, H. Haak, S. Hagemann, J. Jungclaus, S.
9 Marsland, U. Mikolajewicz, and J. Mitchell, 2004: Reconstructing, Monitoring, and
10 Predicting Multi-Decadal-Scale Changes in the North Atlantic Thermohaline Circulation with
11 Sea Surface Temperature. *J. Climate*, **17**, 1605-1614.
12
13 Latif, M., K. Sperber, J. Arblaster, P. Braconnot, D. Chen, A. Colman, U. Cubasch, C.
14 Cooper, P. Delecluse, D. Dewitt, L. Fairhead, G. Flato, T. Hogan, M. Ji, M. Kimoto, A. Kitoh,
15 T. Knutson, H. Le Treut, T. Li, S. Manabe, O. Marti, C. Mechoso, G. Meehl, S. Power, E.
16 Roeckner, J. Sirven, L. Terray, A. Vintzileos, R. Voß, B. Wang, W. Washington, I.
17 Yoshikawa, J. Yu and S. Zebiak, 2001: ENSIP: The El Niño Simulation Intercomparison
18 Project. *Climate Dyn.*, **18**, 255-276.
19
20 Latif, M., T. P. Barnett, M. A. Cane, M., Flugel, N.E. Graham, H. Von Storch, J. S. Xu, and S.
21 E. Zebiak, 1994: A review of ENSO prediction studies. *Climate Dyn.*, **9**, 167–179.
22
23 Levitus, S., T. Boyer, M. Conkright, T. O'Brian, J. Antonov, C. Stephens, S. L. J. D, and R.
24 Gelfeld, 1998: World Ocean Data Base. NOAA Atlas, NESDID18.
25
26 Lin, J.-L., 2007: Interdecadal variability of ENSO in 21 IPCC AR4 coupled GCMs. *Geophys.*
27 *Res. Lett.*, **34**, L12702, doi:10.1029/2006GL028937.

1
2
3
4
5
6
7
8
9
10
11
12
13
14
15
16
17
18
19
20
21
22
23
24
25
26
27

Liu, Z., 2002: A Simple Model Study of ENSO Suppression by External Periodic Forcing. *J. Climate*, **15**, 1088-1098.

Lohmann, K. and M. Latif, 2005: Tropical Pacific Decadal Variability and the Subtropical–Tropical Cells. *J. Climate*, **18**, 5163-5178.

Luo, J.-J., S. Masson, E. Roeckner, G. Madec, and T. Yamagata, 2005: Reducing climatology bias in an ocean-atmosphere CGCM with improved coupling physics. *J. Climate*, **18**, 2344-2360.

Ma, C.-C., C. R. Mechoso, A. W. Robertson, and A. Arakawa, 1996: Peruvian Stratus Clouds and the Tropical Pacific Circulation: A Coupled Ocean-Atmosphere GCM Study. *J. Climate*, **9**, 1635-1645.

Madec, G., 2008: NEMO reference manual, ocean dynamics component: NEMO-OPA. Preliminary version. Note du Pole de modélisation, Institut Pierre-Simon Laplace (IPSL), France, No. 27 ISSN No 1288-1619.

Madec, G., P. Delecluse, M. Imbard, and C. Lévy, 1998: OPA 8.1 Ocean General Circulation Model reference manual. Note du Pole de modélisation, Institut Pierre-Simon Laplace (IPSL), France, No. 11, 91pp.

McPhaden, M. J., Busalacchi, A. J., Cheney, R., Donguy, J. R., Gage, K. S., Halpern, D., Ji, M., Julian, P., Meyers, G., Mitchum, G. T., Niiler, P. P., Picaut, J., Reynolds, R. W., Smith, N., & Takeuchi, K., 1998: The tropical ocean global atmosphere observing system: A decade of progress. *J. Geophys. Res.*, **103** (C7), 14169–14240.

1
2
3
4
5
6
7
8
9
10
11
12
13
14
15
16
17
18
19
20
21
22
23
24
25
26

McPhaden, M. J., S. P. Hayes, L. J. Mangum, and J. M. Toole, 1990: Variability in the western equatorial Pacific Ocean during the 1986-87 El Niño/Southern Oscillation event. *J. Phys. Oceanogr.*, **20**, 190-208.

Meehl, G. A., P. R. Gent, J. M. Arblaster, B. L. Otto-Bliesner, E. C. Brady, et al., 2001: Factors that affect the amplitude of El Nino in global coupled climate models. *Climate Dyn.*, **17**, 515-526.

Navarra, A., et al., 2003: Scale interactions in the climate system: Results from the SINTEX project. *Annals of Geophysics*, **46** (1), 1-171.

Neelin, J. D., D. S. Battisti, A. C. Hirst, F.-F. Jin, Y. Wakata, et al., 1998: ENSO theory *J. Geophys. Res.*, **C7**, 14,261-14,290.

Neelin, J. D., M. Latif, M. A. F. Allaart, M. A. Cane, U. Cubasch, W. L. Gates, P. R. Gent, M. Ghil, C. Gordon, N. C. Lau, C. R. Mechoso, G. A. Meehl, J. M. Oberhuber, S. G. H. Philander, P. S. Schopf, K. R. Sperber, K. R. Sterl, T. Tokioka, J. Tribbia, and S. E. Zebiak, 1992: Tropical air–sea interaction in general circulation models. *Climate Dyn.*, **7**, 73–104.

Neelin, J. D., M. Latif, and F.-F. Jin, 1994: Dynamics of coupled ocean–atmosphere models: The tropical problem. *Annu. Rev. Fluid Mech.*, **26**, 617–659.

Philander, S. G. H., D. Gu, G. Lambert, T. Li, D. Halpern, et al., 1996: Why the ITCZ Is Mostly North of the Equator. *J. Climate*, **9**, 2958-2972.

1 Rayner, N. A., D. E. Parker, E. B. Horton, C. K. Folland, L. V. Alexander, D. P. Rowell, E. C.
2 Kent, and A. Kaplan, 2003: Global analyses of sea surface temperature, sea ice, and night
3 marine air temperature since the late nineteenth century. *J. Geophys. Res.*, **108** (D14), 4407,
4 doi:10.1029/2002JD002670.

5

6 Reynolds, R. W. and T. M. Smith, 1994: Improved global sea surface temperature analyses
7 using optimum interpolation. *J. Climate*, **7**, 929-948.

8

9 Roeckner, E., G. Bäuml, L. Bonaventura, R. Brokopf, M. Esch, M. Giorgetta, S. Hagemann, I.
10 Kirchner, L. Kornblueh, E. Manzini, A. Rhodin, U. Schlese, U. Schulzweida, A. Tompkins,
11 2003: The atmospheric general circulation model ECHAM5. Part I: Model description. Max
12 Planck Institute for Meteorology Rep. 349, 127 pp. [Available from MPI for Meteorology,
13 Bundesstr. 53, 20146 Hamburg, Germany.]

14

15 Roeckner, E., R. Brokopf, M. Esch, M. Giorgetta, S. Hagemann, L. Kornblueh, E. Manzini,
16 U. Schlese, and U. Schulzweida, 2006: Sensitivity of Simulated Climate to Horizontal and
17 Vertical Resolution in the ECHAM5 Atmosphere Model. *J. Climate*, **19**, 3771–3791.

18

19 Schmittner, A., M. Latif, and B. Schneider, 2005: Model projections of the North Atlantic
20 thermohaline circulation for the 21st century assessed by observations. *Geophys. Res. Lett.*,
21 **32**, L23710, doi:10.1029/2005GL024368.

22

23 Schopf, P. S. and M. J. Suarez, 1988: Vacillations in a coupled ocean–atmosphere model. *J.*
24 *Atmos. Sci.*, **45**, 549–566.

25

1 Solomon, A. and D. Zhang, 2006: Pacific Subtropical Cell variability in coupled climate
2 model simulations of the late 19th-20th Century. *Ocean Modelling*, **15**, 236-249,
3 doi:10.1016/j.ocemod.2006.03.007.

4

5 Timmermann, A., J. Oberhuber, A. Bacher, M. Esch, M. Latif, and E. Roeckner, 1999:
6 Increased El Niño frequency in a climate model forced by future greenhouse warming.
7 *Nature*, **398**, 694-697.

8

9 Tompkins, A., 2002: A prognostic parameterization for the subgrid-scale variability of water
10 vapour and clouds in large-scale models and its use to diagnose cloud cover. *J. Atmos. Sci.*, **59**,
11 1917-1942.

12

13 Valcke, S., 2006: OASIS3 user guide. PRISM technical report No.3, 64pp. [Available on
14 <http://www.prism.enes.org>]

15

16 van Oldenborgh, G. J., S. Y. Philip, and M. Collins, 2005: El Niño in a changing climate: a
17 multi-model study. *Ocean Science*, **1**, 81-95.

18

19 Xie, S.-P. and P. A. Arkin, 1997: Global precipitation: A 17-year monthly analysis based on
20 gauge observations, satellite estimates, and numerical model outputs. *Bull. Amer. Meteor.*
21 *Soc.*, **78**, 2539–2558.

22

23 Zebiak, S. E. and M. A. Cane, 1987: A model El Niño–Southern Oscillation. *Mon. Wea. Rev.*,
24 **115**, 2262–2278.

25

1 **Figure Captions**

2

3 Figure 1: Schematic of the Kiel Climate Model. (ECHAM: ECmwf HAMburg atmospheric
4 general circulation model from Max Planck Institute for Meteorology; OASIS: Ocean
5 Atmosphere Sea Ice Soil coupler from CERFACS, European Centre for Research and
6 Advanced Training in Scientific Computation, NEMO: Nucleus for European Modelling of
7 the Ocean from LOCEAN - Institut Pierre Simon Laplace; OPA: Océan PARallélisé ; LIM:
8 Louvain-la-Neuve Ice model)

9

10 Figure 2: Global mean 2-m air temperatures [$^{\circ}\text{C}$] of control (20C, black) and 8 members of
11 global warming experiments (21C, colors) started from different initial conditions. CO_2
12 concentration is increased at 1% per year till doubling and then stabilized for the 21C
13 experiments.

14

15 Figure 3: Sea surface temperature bias [$^{\circ}\text{C}$] of 20C control simulation averaged over last 100
16 yrs referenced to observation (Reynolds and Smith, 1994).

17

18 Figure 4: Annual mean of (a-b) eastward zonal wind stress [10^{-2} Pa], (c-d) wind stress (arrow)
19 [10^{-1} Pa] and its curl [10^{-8} N/m^3], and (e-f) precipitation [mm/day] of the 20C control
20 simulation (left panels) and observations (right panels).

21

22 Figure 5: Annual mean of (a-b) vertical temperature [$^{\circ}\text{C}$] section along the equator and (c-d)
23 20°C isotherm depth [m] of the 20C control simulation (20C, left panels) and observations
24 (right panels). (e) Streamfunction, Ψ [$\text{Sv}=10^6$ m^3/s] over the Pacific domain from coupled run
25 and (f) that from CORE-forced standalone ocean model.

26

1 Figure 6: Hovmoeller diagram of sea surface temperature anomalies [$^{\circ}\text{C}$] along the equatorial
2 Pacific from (a) the 20C control simulation and (b) observations (HadISST, 1870-2004).

3

4 Figure 7: Standard deviation of sea surface temperature anomalies [$^{\circ}\text{C}$] from (a) the 20C
5 control simulation (330yrs) and (b) observations (HadISST, 1870-2004).

6

7 Figure 8: Niño3 SST anomaly [$^{\circ}\text{C}$] time series of (a) 20C control simulation and (b)
8 observations (HadISST, 1870-2004), and corresponding (c) spectra [$^{\circ}\text{C}^2$] and (d) monthly
9 standard deviations [$^{\circ}\text{C}$] (black: observation, blue: model).

10

11 Figure 9: Anomalies along the equator of (a, d) 10-m eastward zonal wind speed [m/s], (b, e)
12 20°C isotherm depth [m], and (c, f) SST [$^{\circ}\text{C}$] from (upper) the 20C control simulation and
13 (lower) observations (TOGA-TAO; McPhaden et al. 1998), respectively.

14

15 Figure 10: Regression (shading) and explained variance (contour) of monthly anomalies of
16 Niño3 SST onto sea level pressure (hPa/ $^{\circ}\text{C}$): (a) 20C control simulation (330 years) and (b)
17 observations (55 years of NCEP/NCAR reanalysis sea level pressure and HadISST Niño3
18 SST).

19

20 Figure 11: Ensemble mean response of surface temperature [$^{\circ}\text{C}$] from the eight members of
21 21C global warming experiments. Last 30 years (year 71-100) from 21C experiments are used
22 for the calculation.

23

24 Figure 12: Ensemble mean responses (last 30 years of 21C experiments) of (a) temperature
25 [$^{\circ}\text{C}$] along the equator, (b) Pacific streamfunction, Ψ [Sv], (c) wind stress (arrow) [2×10^{-2} Pa]
26 and its curl [10^{-8} N/m³], and (d) 20°C isotherm depth [m].

27

1 Figure 13: Evolution of (a) tropical- and (b) subtropical cell indices [Sv] of 20C control (thick
2 black lines) and 21C global warming experiments (thick red lines). Thick lines represent 11-yr
3 running averaged ensemble mean and thin lines annual values of the ensemble members.
4 Tropical and subtropical cell index, which represent strength of off-equatorial circulation, are
5 defined as $\Psi_{\max}(5^{\circ}\text{S}-5^{\circ}\text{N}, \text{upper } 250\text{m}) - \Psi_{\min}(5^{\circ}\text{S}-5^{\circ}\text{N}, \text{upper } 250\text{m})$ and $\Psi_{\max}(10^{\circ}\text{N}-30^{\circ}\text{N},$
6 $\text{upper } 250\text{m}) - \Psi_{\min}(10^{\circ}\text{S}-30^{\circ}\text{S}, \text{upper } 250\text{m})$, respectively. (c) Maximum streamfunction
7 [Sv] of Northern Hemisphere subtropical cell and (d) minimum streamfunction of Southern
8 Hemisphere subtropical cell (note that minimum streamfunction for southern hemisphere
9 indicates maximum poleward streamfunction; ref. Fig 5e).

10

11 Figure 14: Evolution of Niño3 SST anomalies [$^{\circ}\text{C}$] from the eight members of 21C
12 experiments. The thick line represents the ensemble mean smoothed with a 10-year running
13 mean filter.

14

15 Figure 15: Ensemble mean spectra [$^{\circ}\text{C}^2$] of Niño3 SST anomalies. Spectra are computed from
16 last 30 years the 21C experiments (after removing the linear trend) and eight non-overlapping
17 30 years chunks from the 20C control simulation. Bars indicate the one standard deviation
18 range derived from the 8 individual members.

19

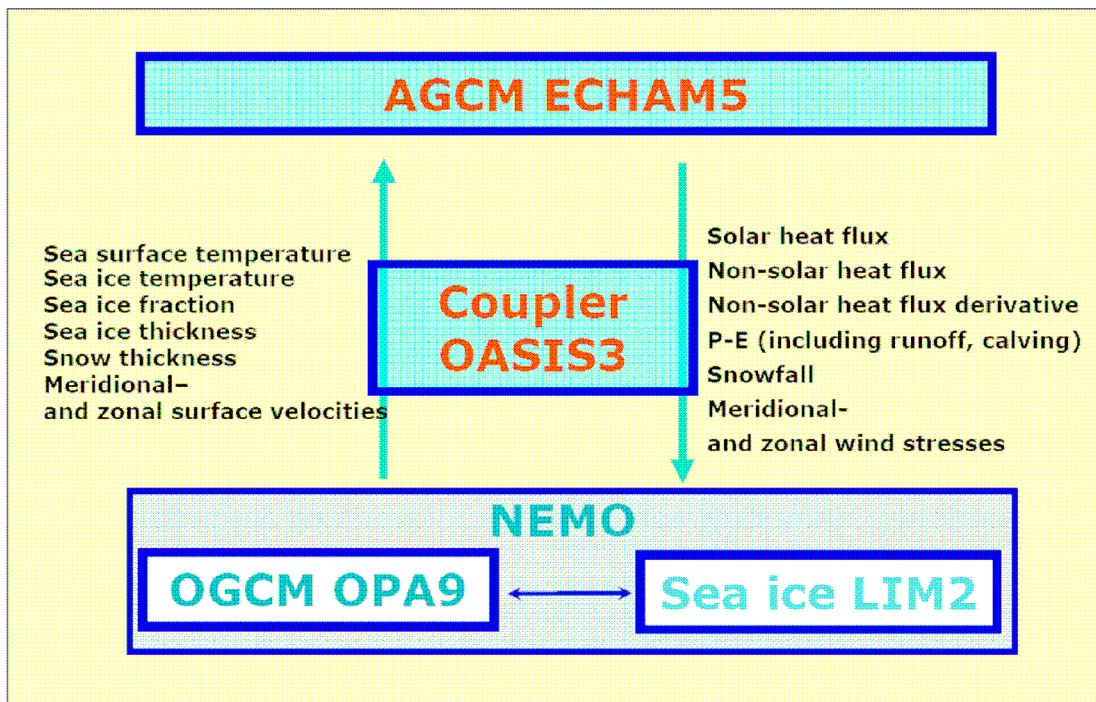
20 Figure 16: (a) Histograms of monthly Niño3 SST anomalies and (b) annual cycle (yearly
21 mean removed) of Niño3 SST [$^{\circ}\text{C}$]. Periods of analysis of 20C (blue) and 21C (red)
22 experiments are described in Fig. 15. Observations (black, HadISST 1870-2004) are shown
23 for comparison.

24

25 Figure 17: Scatter plots and linear regression results for the feedback changes. (a, b)
26 anomalies of Niño3 Z_{20} and SST, (c, d) anomalies of Niño3 SST and Niño4 wind stresses. (a,
27 c) for 20C, (b, d) for 21C experiments, respectively.

1 **Figures**

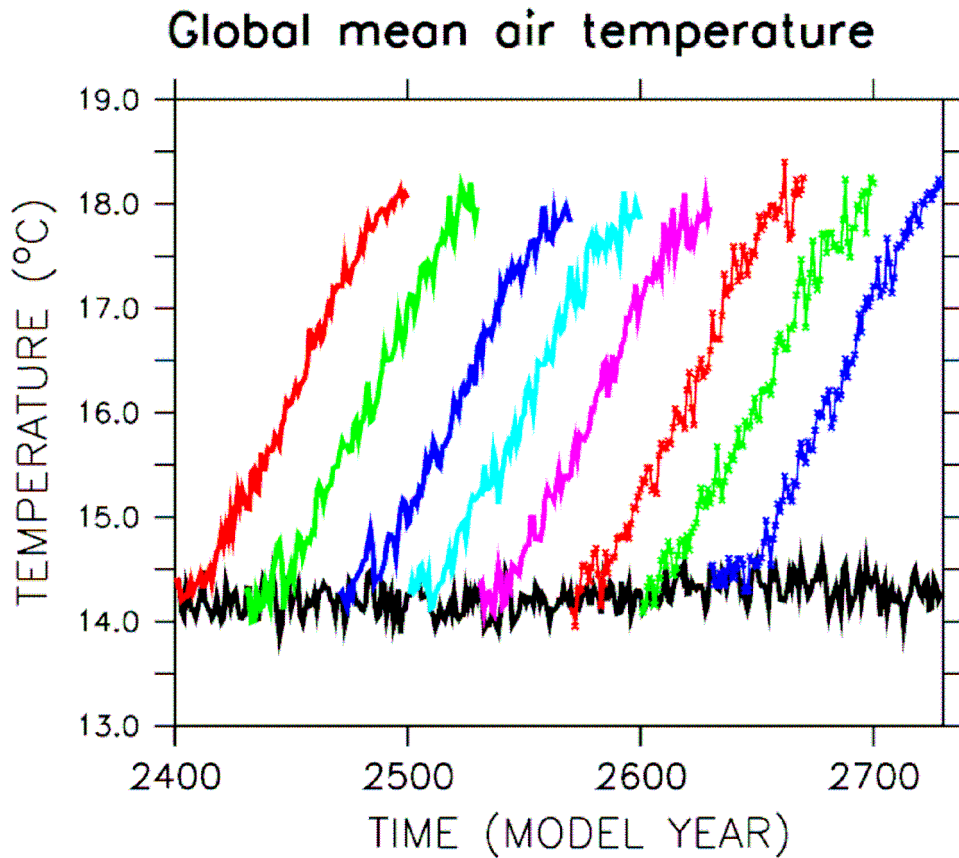
2



3

4 Figure 1: Schematic of the Kiel Climate Model. (ECHAM: ECmwf HAMburg atmospheric
5 general circulation model from Max Planck Institute for Meteorology; OASIS: Ocean
6 Atmosphere Sea Ice Soil coupler from CERFACS, European Centre for Research and
7 Advanced Training in Scientific Computation, NEMO: Nucleus for European Modelling of
8 the Ocean from LOCEAN - Institut Pierre Simon Laplace; OPA: Océan PARallélisé ; LIM:
9 Louvain-la-Neuve Ice model)

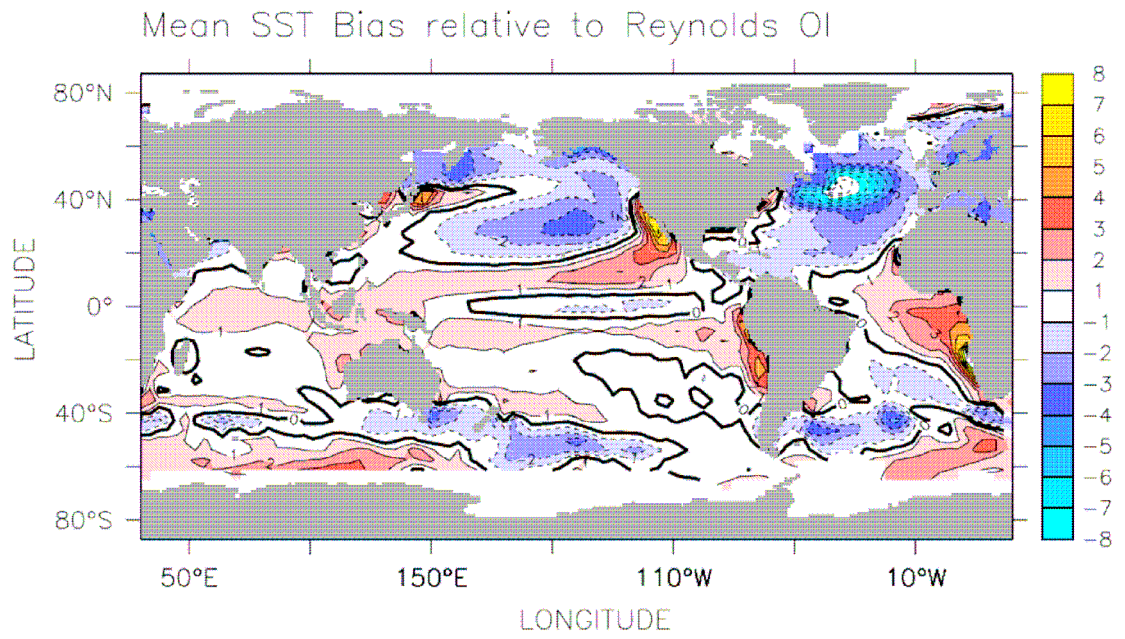
10



1

2 Figure 2: Global mean 2-m air temperatures [°C] of control (20C, black) and 8 members of
3 global warming experiments (21C, colors) started from different initial conditions. CO₂
4 concentration is increased at 1% per year till doubling and then stabilized for the 21C
5 experiments.

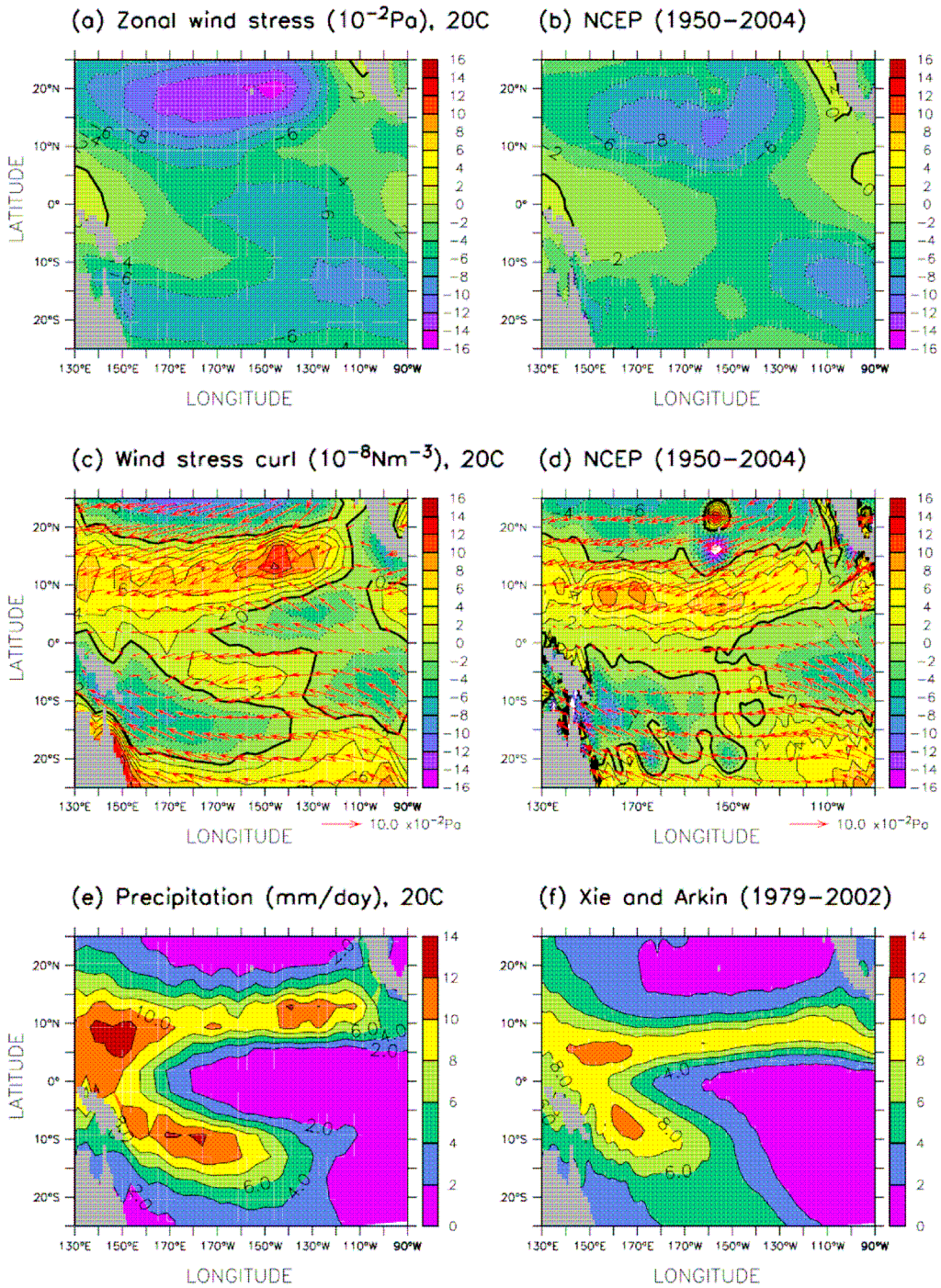
6



1

2 Figure 3: Sea surface temperature bias [°C] of 20C control simulation averaged over last 100
3 yrs referenced to observation (Reynolds and Smith, 1994).

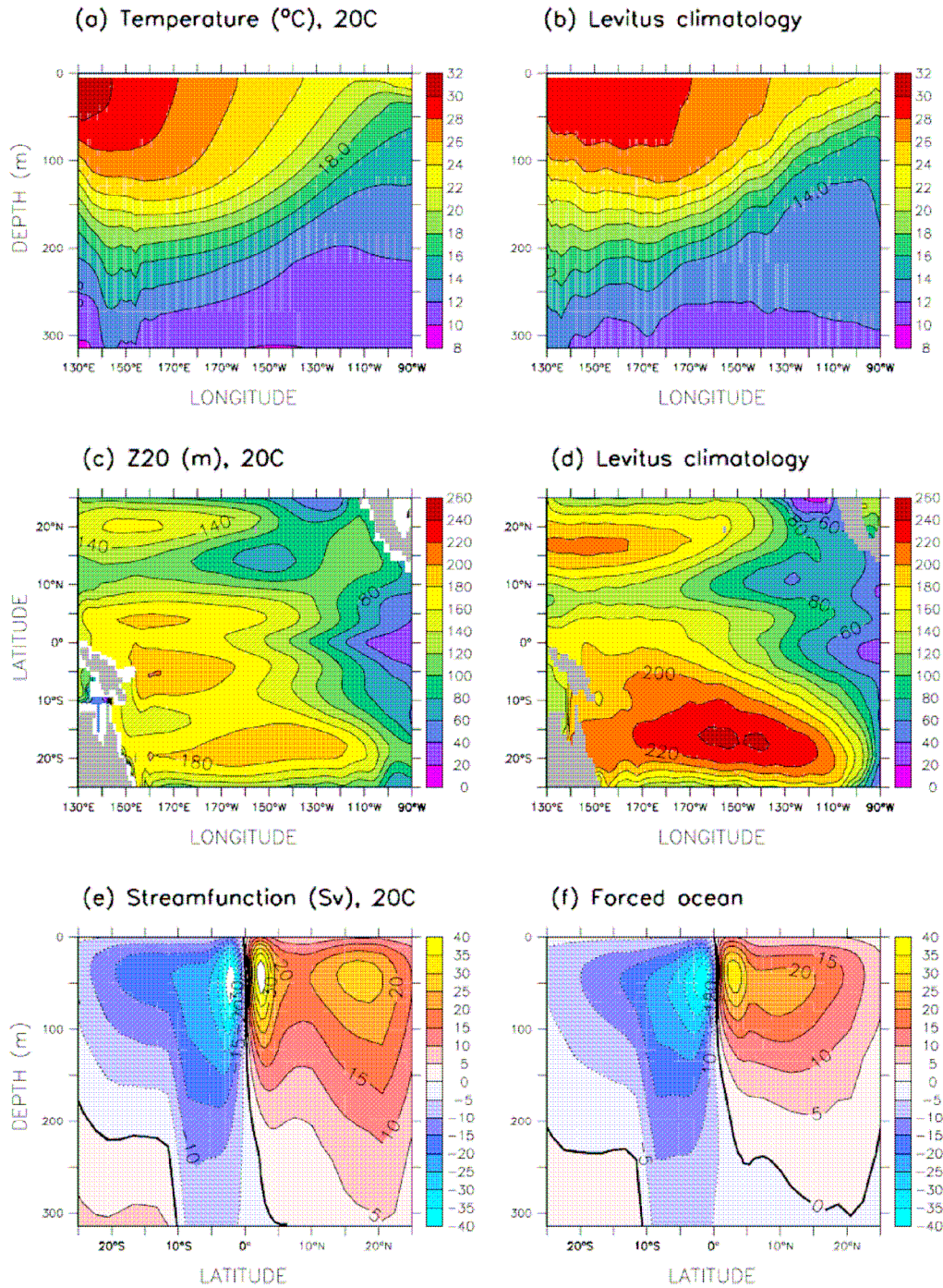
4



1

2 Figure 4: Annual mean of (a-b) eastward zonal wind stress [10^{-2} Pa], (c-d) wind stress (arrow)
 3 [10^{-1} Pa] and its curl [10^{-8} N/m³], and (e-f) precipitation [mm/day] of the 20C control
 4 simulation (left panels) and observations (right panels).

5



1

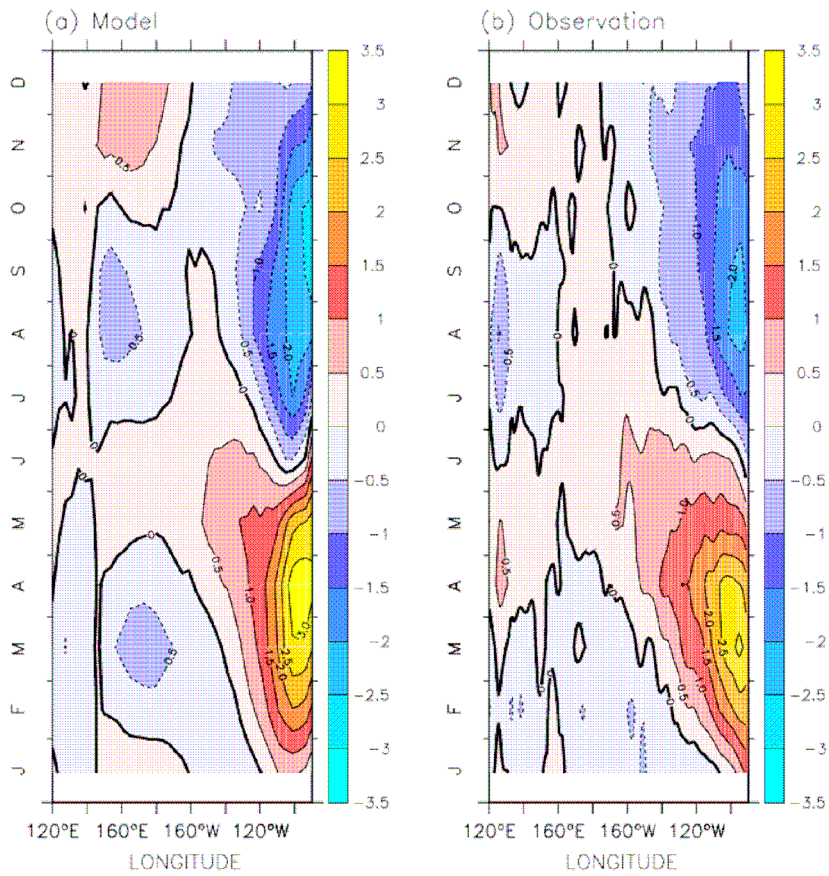
2 Figure 5: Annual mean of (a-b) vertical temperature [°C] section along the equator and (c-d)

3 20°C isotherm depth [m] of the 20C control simulation (20C, left panels) and observations

4 (right panels). (e) Streamfunction, Ψ [$\text{Sv}=10^6 \text{ m}^3/\text{s}$] over the Pacific domain from coupled run

5 and (f) that from CORE-forced standalone ocean model.

6

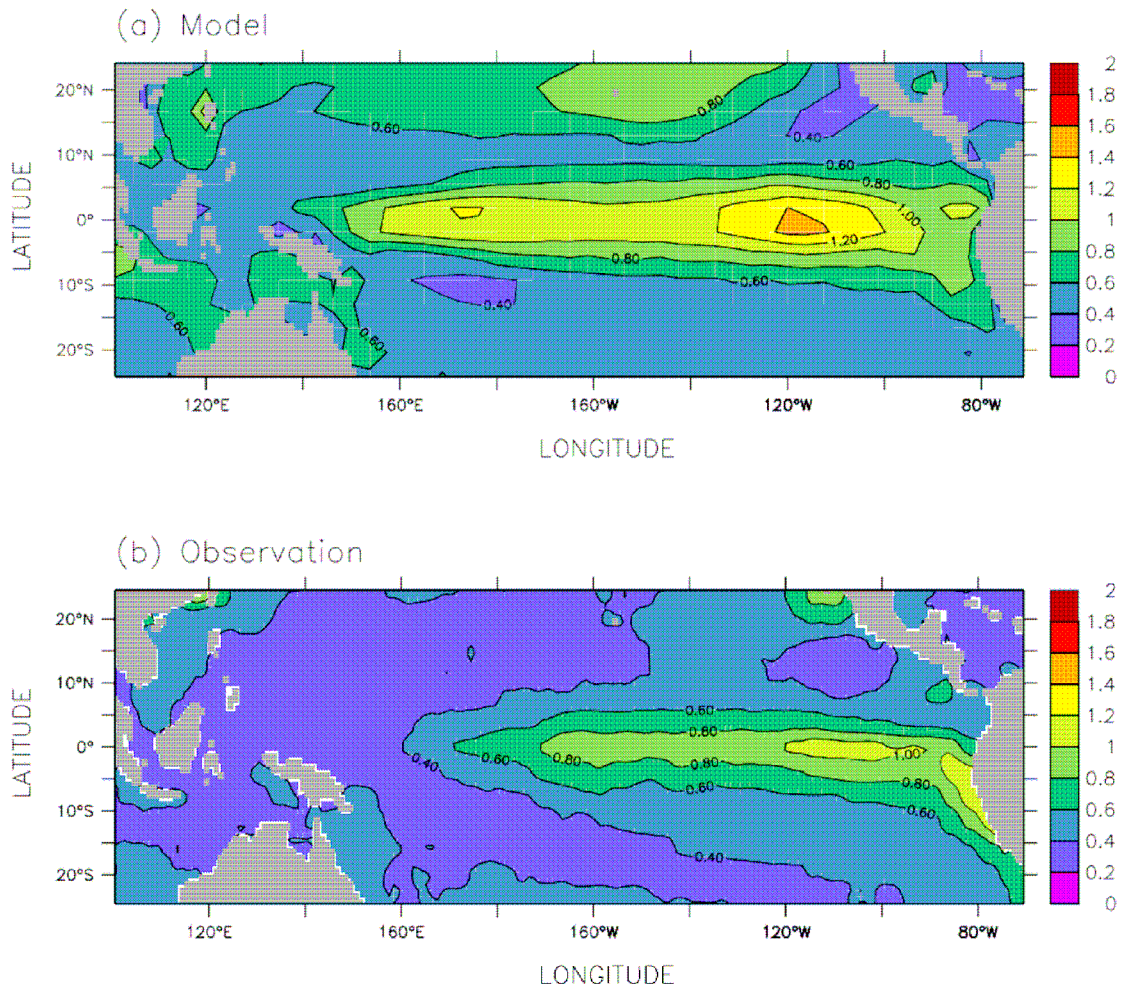


1

2 Figure 6: Hovmoeller diagram of sea surface temperature anomalies [$^{\circ}\text{C}$] along the equatorial

3 Pacific from (a) the 20C control simulation and (b) observations (HadISST, 1870-2004).

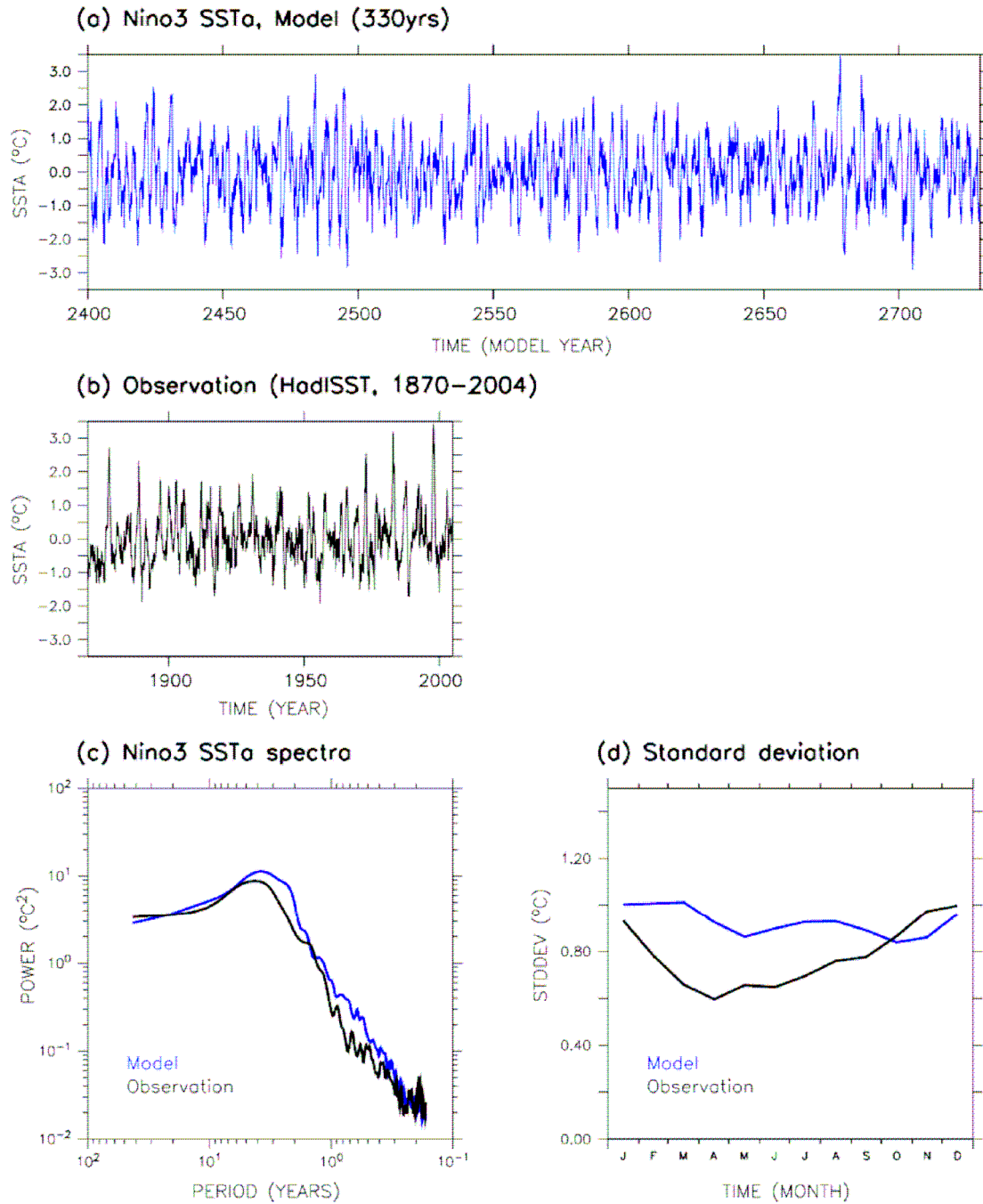
4



1

2 Figure 7: Standard deviation of sea surface temperature anomalies [$^{\circ}\text{C}$] from (a) the 20C
 3 control simulation (330yrs) and (b) observations (HadISST, 1870-2004).

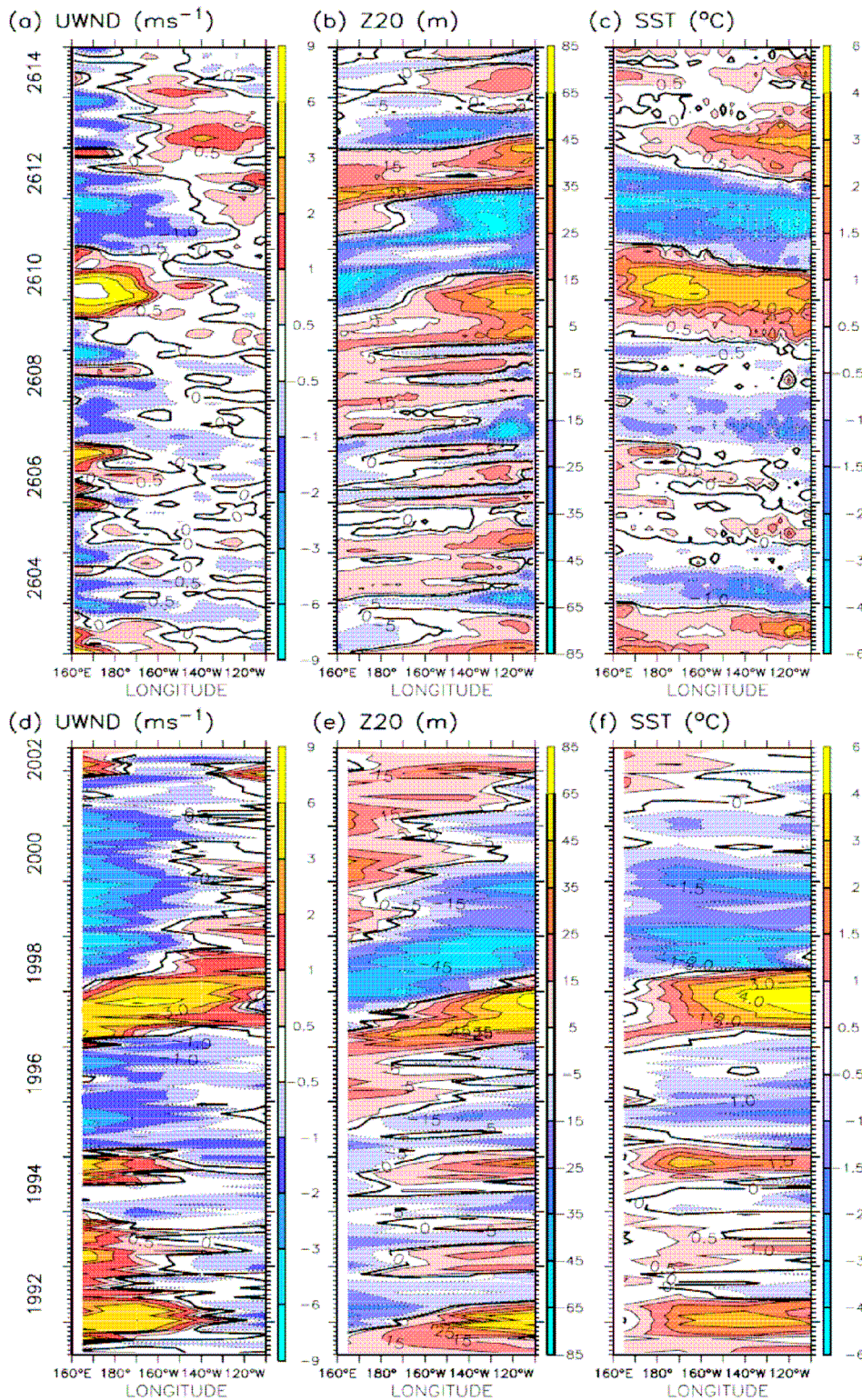
4



1

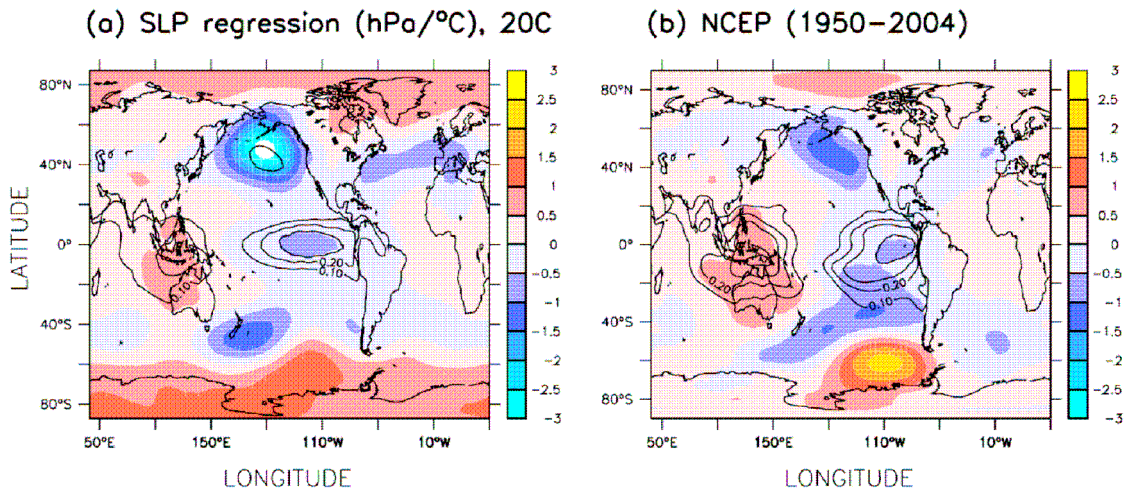
2 Figure 8: Niño3 SST anomaly [$^{\circ}\text{C}$] time series of (a) 20C control simulation and (b)
 3 observations (HadISST, 1870-2004), and corresponding (c) spectra [$^{\circ}\text{C}^2$] and (d) monthly
 4 standard deviations [$^{\circ}\text{C}$] (black: observation, blue: model).

5



1

2 Figure 9: Anomalies along the equator of (a, d) 10-m eastward zonal wind speed [m/s], (b, e)
 3 20°C isotherm depth [m], and (c, f) SST [$^{\circ}\text{C}$] from (upper) the 20C control simulation and
 4 (lower) observations (TOGA-TAO; McPhaden et al. 1998), respectively.



1

2 Figure 10: Regression (shading) and explained variance (contour) of monthly anomalies of

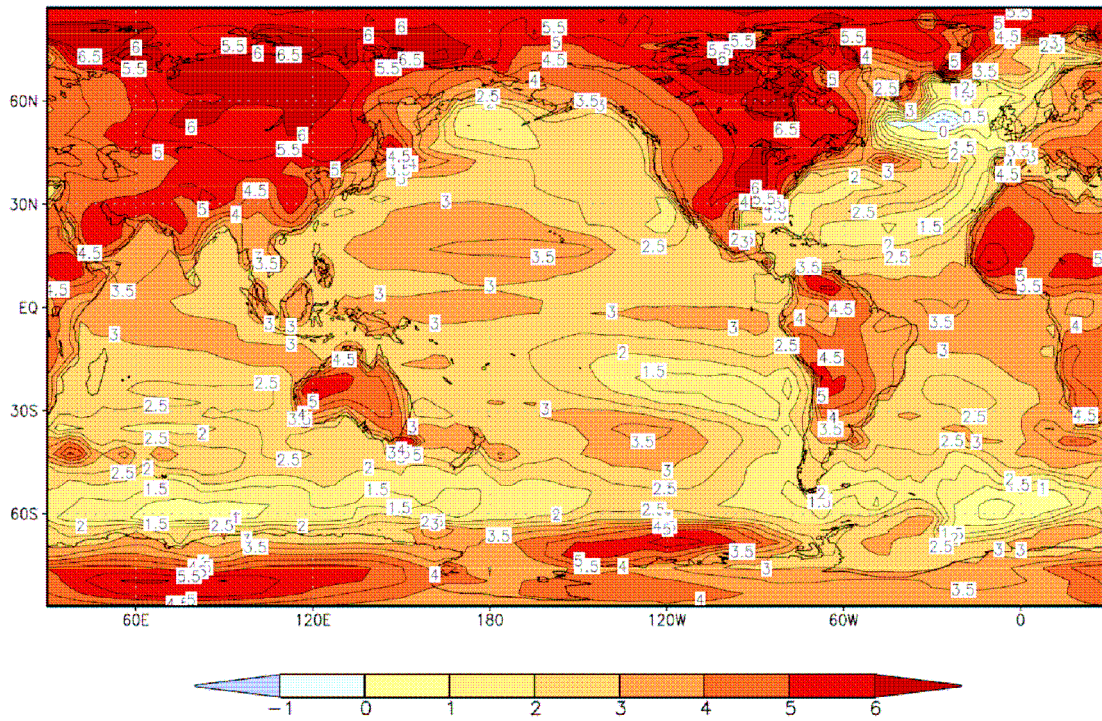
3 Niño3 SST onto sea level pressure (hPa/°C): (a) 20C control simulation (330 years) and (b)

4 observations (55 years of NCEP/NCAR reanalysis sea level pressure and HadISST Niño3

5 SST).

6

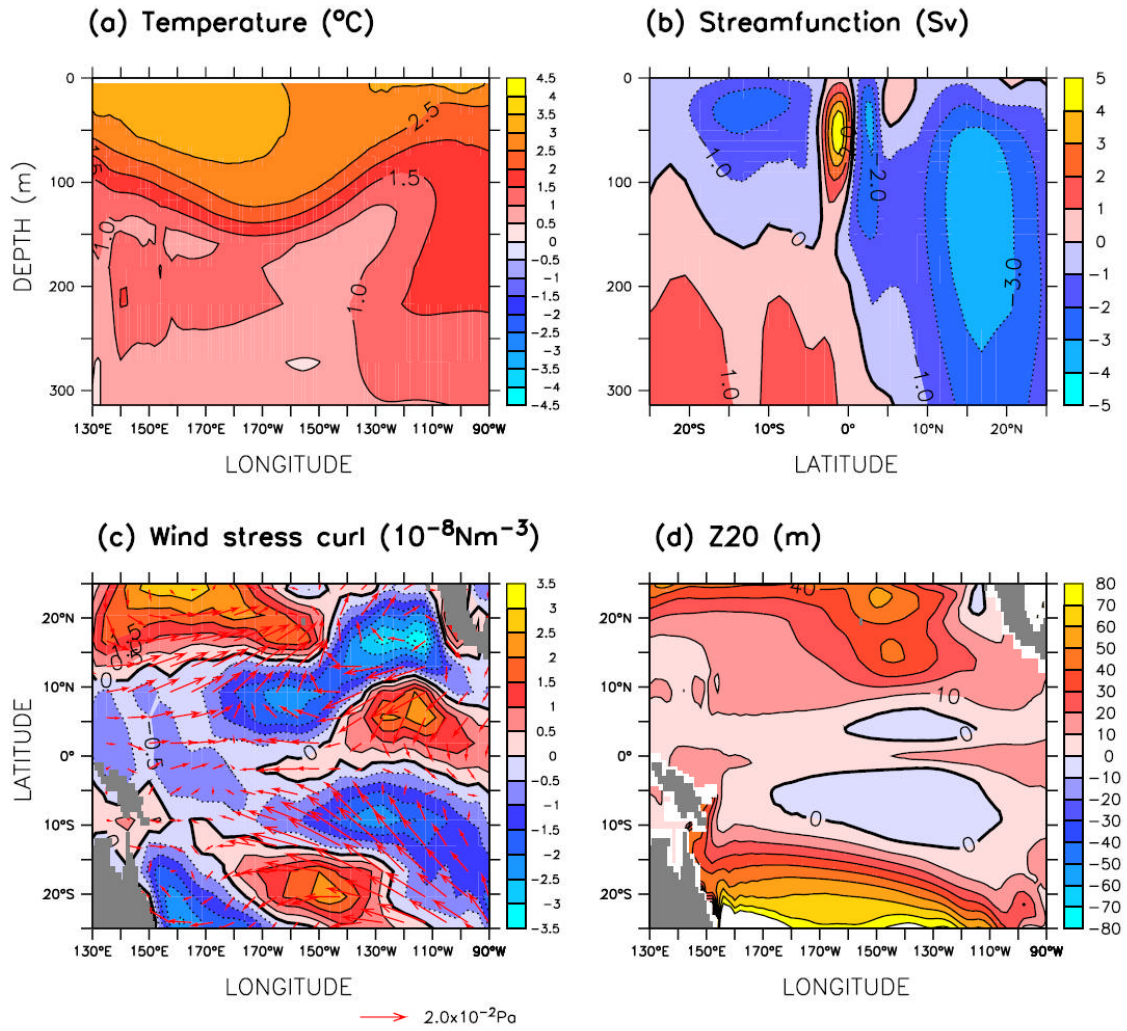
Surface temperature response



1

2 Figure 11: Ensemble mean response of surface temperature [$^{\circ}\text{C}$] from the eight members of
3 21C global warming experiments. Last 30 years (year 71-100) from 21C experiments are used
4 for the calculation.

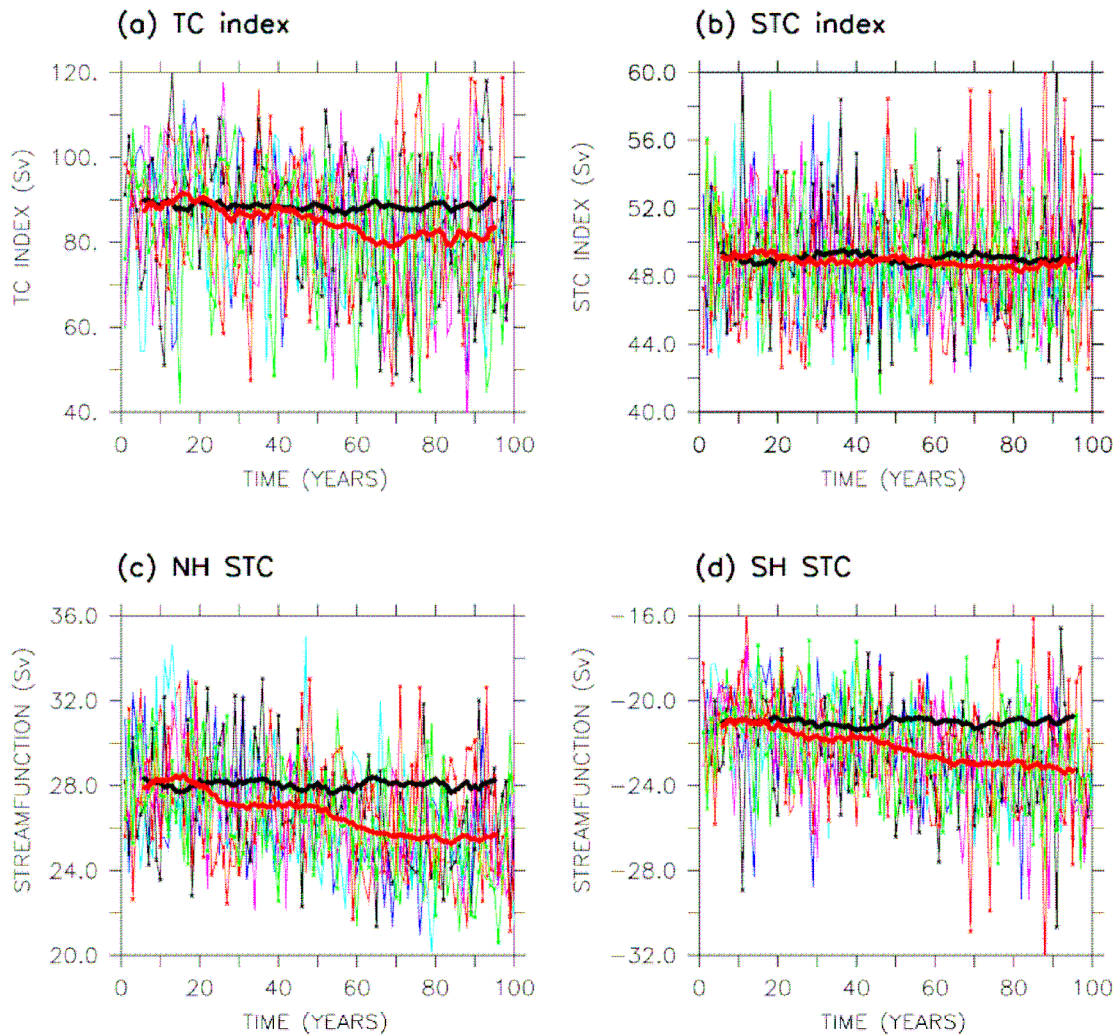
5



1

2 Figure 12: Ensemble mean responses (last 30 years of 21C experiments) of (a) temperature
 3 [°C] along the equator, (b) Pacific streamfunction, Ψ [Sv], (c) wind stress (arrow) [2×10^{-2} Pa]
 4 and its curl [10^{-8} N/m³], and (d) 20°C isotherm depth [m].

5

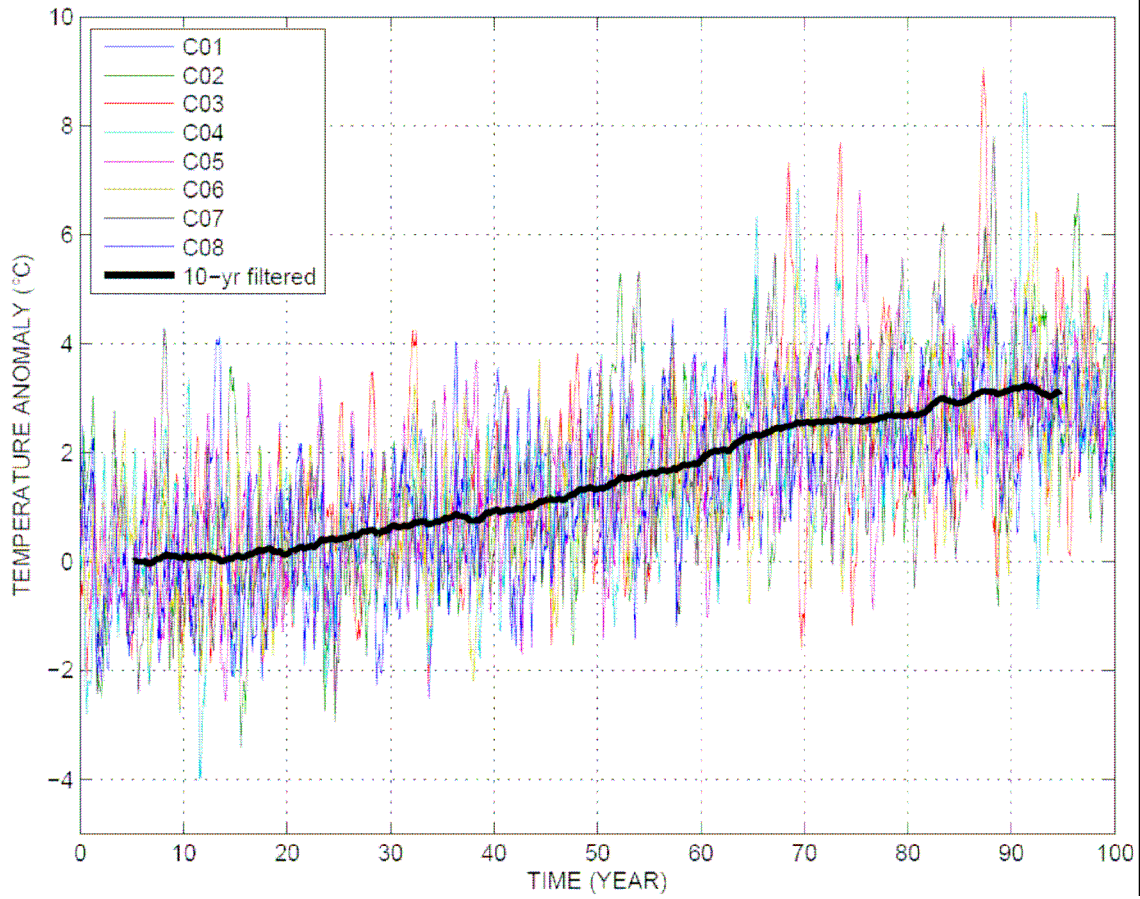


1

2 Figure 13: Evolution of (a) tropical- and (b) subtropical cell indices [Sv] of 20C control (thick
 3 black lines) and 21C global warming experiments (thick red lines). Thick lines represent 11-yr
 4 running averaged ensemble mean and thin lines annual values of the ensemble members.

5 Tropical and subtropical cell index, which represent strength of off-equatorial circulation, are
 6 defined as $\Psi_{\max}(5^{\circ}\text{S}-5^{\circ}\text{N}, \text{upper } 250\text{m}) - \Psi_{\min}(5^{\circ}\text{S}-5^{\circ}\text{N}, \text{upper } 250\text{m})$ and $\Psi_{\max}(10^{\circ}\text{N}-30^{\circ}\text{N},$
 7 $\text{upper } 250\text{m}) - \Psi_{\min}(10^{\circ}\text{S}-30^{\circ}\text{S}, \text{upper } 250\text{m})$, respectively. (c) Maximum streamfunction
 8 [Sv] of Northern Hemisphere subtropical cell and (d) minimum streamfunction of Southern
 9 Hemisphere subtropical cell (note that minimum streamfunction for southern hemisphere
 10 indicates maximum poleward streamfunction; ref. Fig 5e).

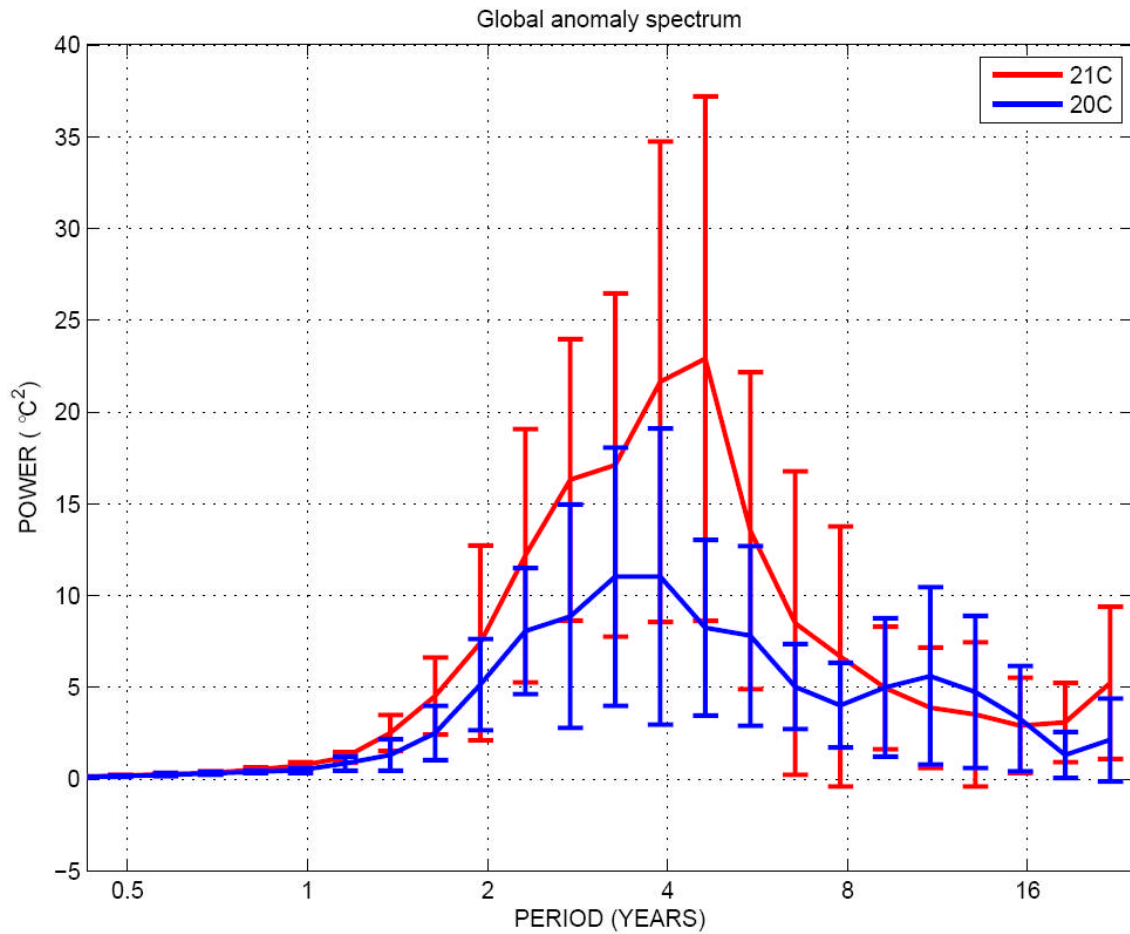
11



1

2 Figure 14: Evolution of Niño3 SST anomalies [°C] from the eight members of 21C
3 experiments. The thick line represents the ensemble mean smoothed with a 10-year running
4 mean filter.

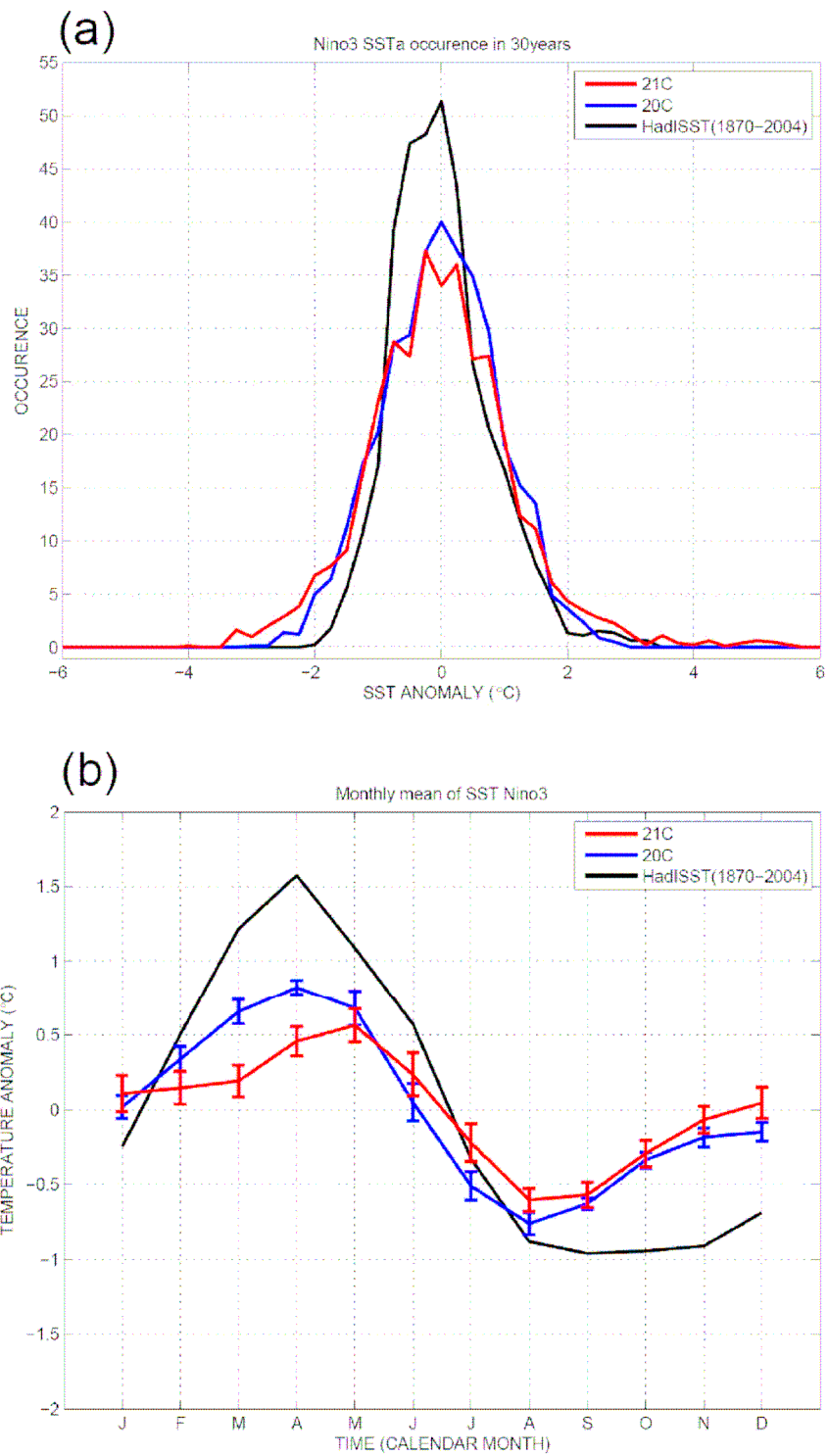
5



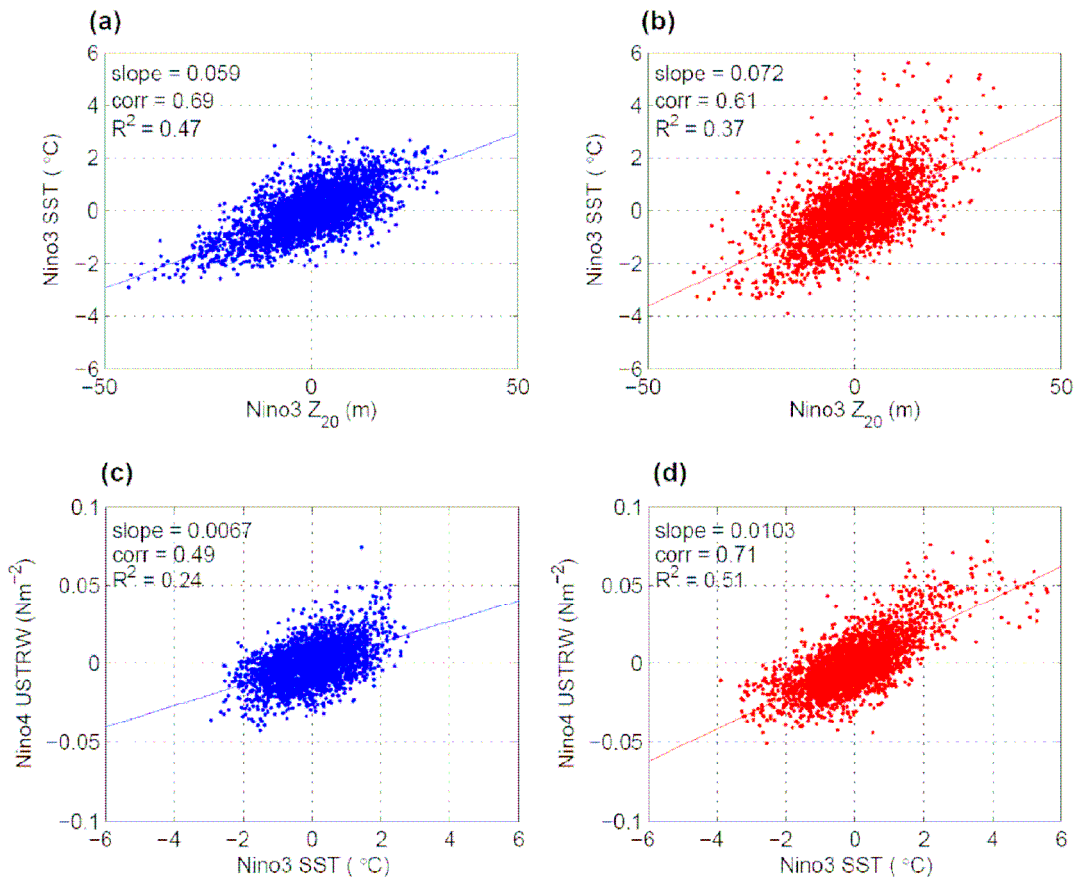
1

2 Figure 15: Ensemble mean spectra [$^{\circ}\text{C}^2$] of Niño3 SST anomalies. Spectra are computed from
 3 last 30 years the 21C experiments (after removing the linear trend) and eight non-overlapping
 4 30 years chunks from the 20C control simulation. Bars indicate the one standard deviation
 5 range derived from the 8 individual members.

6



1
 2 Figure 16: (a) Histograms of monthly Niño3 SST anomalies and (b) annual cycle (yearly
 3 mean removed) of Niño3 SST [°C]. Periods of analysis of 20C (blue) and 21C (red)
 4 experiments are described in Fig. 15. Observations (black, HadISST 1870-2004) are shown
 5 for comparison.



1

2 Figure 17: Scatter plots and linear regression results for the feedback changes. (a, b)

3 anomalies of Niño3 Z₂₀ and SST, (c, d) anomalies of Niño3 SST and Niño4 wind stresses. (a,

4 c) for 20C, (b, d) for 21C experiments, respectively.

5